

Unconventional Array Design in the Autocorrelation Domain

- Isophoric *ID* Thinning

L. Poli,⁽¹⁾⁽²⁾ *Senior Member, IEEE*, G. Oliveri,⁽¹⁾⁽²⁾ *Fellow, IEEE*, N. Anselmi,⁽¹⁾⁽²⁾ *Senior Member, IEEE*, A. Benoni,⁽¹⁾ *Member, IEEE*, L. Tosi,⁽¹⁾ *Member, IEEE*, and A. Massa,⁽¹⁾⁽²⁾⁽³⁾⁽⁴⁾⁽⁵⁾ *Fellow, IEEE*

⁽¹⁾ *ELEDIA Research Center (ELEDIA@UniTN - University of Trento)*

DICAM - Department of Civil, Environmental, and Mechanical Engineering

Via Mesiano 77, 38123 Trento - Italy

E-mail: {lorenzo.poli, giacomo.oliveri, nicola.anselmi.1, arianna.benoni, luca.tosi-1, andrea.massa}@unitn.it;

Website: www.eledia.org/eledia-unitn

⁽²⁾ *CNIT - "University of Trento" ELEDIA Research Unit*

Via Mesiano 77, 38123 Trento - Italy

Website: www.eledia.org/eledia-unitn

⁽³⁾ *ELEDIA Research Center (ELEDIA@UESTC - UESTC)*

School of Electronic Science and Engineering, Chengdu 611731 - China

E-mail: andrea.massa@uestc.edu.cn

Website: www.eledia.org/eledia-uestc

⁽⁴⁾ *ELEDIA Research Center (ELEDIA@TSINGHUA - Tsinghua University)*

30 Shuangqing Rd, 100084 Haidian, Beijing - China

E-mail: andrea.massa@tsinghua.edu.cn

Website: www.eledia.org/eledia-tsinghua

⁽⁵⁾ *School of Electrical Engineering*

Tel Aviv University, Tel Aviv 69978 - Israel

E-mail: andrea.massa@eng.tau.ac.il

Website: <https://engineering.tau.ac.il/>

This work has been submitted to the IEEE for possible publication. Copyright may be transferred without notice, after which this version may no longer be accessible.

Unconventional Array Design in the Autocorrelation Domain

- Isophoric *ID* Thinning

L. Poli, G. Oliveri, N. Anselmi, A. Benoni, L. Tosi, and A. Massa

Abstract

The synthesis of thinned isophoric arrays (*TIAs*) radiating mask-constrained patterns is addressed. By leveraging on the recently-introduced formulation of the design of antenna arrays in the autocorrelation-domain (*AD*), the *TIA* synthesis is recast as the matching of a target autocorrelation function derived from the user-defined guidelines and objectives. By exploiting the autocorrelation invariance of cyclic binary sequences, the *AD* solution space is significantly reduced and it is efficiently sampled by means of a discrete hybrid optimization approach. Two possible implementations of the *AD*-based *TIA* formulation are discussed and assessed in a set of representative numerical examples concerned with both ideal and real radiators, which are full-wave modeled to account for the mutual coupling effects. Comparisons with traditional pattern-domain (*PD*) synthesis methods are also considered to point out the features and the advantages of *AD*-based approaches.

Key words: Isophoric arrays, linear arrays, thinned arrays, optimization methods.

1 Introduction and Motivations

Unconventional (antenna) arrays (*UAs*) are emerging as a key enabling technology across several applicative domains including satellite and terrestrial communications, automotive radar and sensing, far-field and near-field imaging, direction-of-arrival estimation, and localization [1]-[7]. The success of *UAs* is motivated by the possibility to overcome the limitations of traditional (i.e., conventional) architectures in terms of radiation performance, flexibility, and fabrication complexity [1]-[7]. Within *UAs*, thinned isophoric arrays (*TIAs*) [3][8]-[13] have been proposed as a competitive solution for the simultaneous minimization of both the cost and the weight of the antenna system, while still radiating suitable power patterns [1]. Moreover, *TIAs* may potentially accommodate multiple co-existing functionalities or services on the same physical antenna aperture through interleaving [14][15].

Unfortunately, these advantages are yielded with more complex mechanisms to control/adjust the features of the radiation pattern with respect to other classes of both traditional/conventional and unconventional array layouts [1] because of (i) the reduced number of degrees-of-freedom (*DoFs*) and (ii) the discrete, non-linear, and multi-minima nature of the associated design/pattern control problem [1][16]-[18].

In the state-of-the-art literature, a wide variety of design methods has been proposed to effectively control the pattern features of *TIAs*. Low-complexity strategies based on statistical techniques have been initially investigated owing to their efficiency, also dealing with very wide apertures, but they only allow the prediction/control of a limited set of radiation features [e.g., the average sidelobe level (*SLL*)] [8][19]. Evolutionary global optimization techniques have been exploited [3][9][10][20]-[23], as well, but they may suffer from slow convergence and generally imply a heavy computational burden when synthesizing large *TIAs* [24]. The use of analytical techniques has been considered to circumvent these issues, which are related to high-dimensional solution spaces [11][12], as well as their hybridization with optimization techniques to combine the advantages of both concepts [16][17], but the beam control still turned out to be limited (i.e., only the reduction of the *SLL* has been usually yielded) [11][12]. Recently, an innovative paradigm has been introduced that reformulates the array synthesis problem from the pattern domain (*PD*) to a transformed domain [25], namely the *autocorre-*

lation domain (*AD*) [25], by taking advantage of the analytical relationships between the autocorrelation of the array excitations and the associated power pattern samples. Starting from binary sequences with known redundancy properties, closed-form synthesis expressions have been derived that *a-priori* guarantee to obtain *TIA*s layouts fulfilling user-defined specifications on the *SLL*, the directivity, the half-power beam-width, and the power pattern along user-defined directions [25]. Notwithstanding the solid theoretical foundation, its efficiency, and its effectiveness, such a *TIA*-oriented design process [25] has some basic limitations since it (*i*) relies on the availability of analytical sequences with known autocorrelation features, thus it is severely constrained to a reduced set of geometries and thinning factors [25], and (*ii*) does not allow the user to define arbitrary beam shaping / sidelobe profiles, the pattern properties being mostly dictated by the class of analytical sequences at hand [25].

By leveraging on the theoretical framework developed in [25], the objective of this work is to define an innovative general-purpose synthesis method where the design of a *TIA*s affording user-defined beam-shapes is recast as the matching of suitable autocorrelation functions without the need of auxiliary analytical binary sequences. More specifically, the setup of *TIA* layouts matching the user-defined synthesis objectives (e.g., compliance with a mask) is firstly reformulated as a combinatorial problem in the *AD*. By exploiting the cyclic periodicity property of the autocorrelation function of discrete sequences [11], the solution space of the arising *AD* problem is significantly reduced and it is successively sampled with a hybrid global/local evolutionary optimization technique.

To the best of the authors' knowledge, the novelty of our work over existing literature includes (*i*) the introduction of a generalized formulation of *TIA* synthesis problems in the *AD* that, unlike previous *AD*-based approaches, allows the designer to set arbitrary pattern constraints without the need of auxiliary analytical binary sequences, by also reducing the dimensionality of the solution space with respect to standard *PD* techniques; (*ii*) the derivation of two innovative implementations of the *AD* formulation based on either the "Mask Equality" (*ME*) strategy or the "Feasible Pattern Equality" (*FPE*) one.

The outline of the paper is as follows. The formulation of the *TIA* synthesis problem in the *AD* is discussed in Sect. 2, while Section 3 details the solution process based on an evolutionary

optimizer. Afterwards, a representative set of numerical experiments is illustrated to assess the features and the potentialities of the proposed *TIA* synthesis method also in comparison with state-of-the-art thinning techniques (Sect. 4). Conclusions and final remarks follow (Sect. 5).

2 *TIA* Synthesis Formulation

Let us consider a linear *TIA* of N elements [Fig. 1(a)] arranged along the $\hat{\mathbf{z}}$ direction in a regular grid of P ($P > N$) candidate locations, $\{(x_p, y_p, z_p) = (0, 0, d_p); p = 0, \dots, P - 1\}$, where

$$d_p = \left(p - \frac{P-1}{2}\right) \times \Delta z, \quad (1)$$

Δz being the grid step. Such a *TIA* is univocally described by the *TIA descriptor vector* $\boldsymbol{\alpha}$ [$\boldsymbol{\alpha} \in \mathcal{D}(\boldsymbol{\alpha})$, $\mathcal{D}(\boldsymbol{\alpha})$ being the solution space] whose p -th ($p = 0, \dots, P - 1$) entry, α_p , is a binary value ($\alpha_p = 1/0$ if the p -th grid location is occupied/empty) and $N = \sum_{p=0}^{P-1} \alpha_p$. Moreover, the radiated power pattern [2]⁽¹⁾ turns out to be

$$\mathcal{E}(u; \boldsymbol{\alpha}) \triangleq \left| \sum_{p=0}^{P-1} \alpha_p F_p(u) \exp\left(j \frac{2\pi d_p}{\lambda} u\right) \right|^2 \quad (2)$$

where λ is the wavelength and $F_p(u)$ is the p -th ($p = 0, \dots, P - 1$) embedded element pattern. According to this notation, the problem of synthesizing a *TIA* with mask-constrained beam features can be then stated in the (traditional) *PD* as follows

Pattern-Domain TIA (PD-TIA) Design Problem - Find $\boldsymbol{\alpha}^{opt}$ [$\boldsymbol{\alpha}^{opt} \in \mathcal{D}(\boldsymbol{\alpha})$] such that

$$\tilde{\mathcal{E}}(u; \boldsymbol{\alpha}^{opt}) \leq \mathcal{M}(u) \quad (3)$$

within the visible range $u \in [-1, 1]$.

In (3), $\tilde{\mathcal{E}}(u; \boldsymbol{\alpha})$ is the *TIA* normalized power pattern,

$$\tilde{\mathcal{E}}(u; \boldsymbol{\alpha}) \triangleq \frac{\mathcal{E}(u; \boldsymbol{\alpha})}{\mathcal{E}(0; \boldsymbol{\alpha})}, \quad (4)$$

⁽¹⁾For the sake of notation simplicity, single-polarization antennas are hereinafter considered. However, double polarization radiators can be straightforwardly taken into account within the same theoretical framework by introducing co/cross polar masks.

$u = \cos \theta$, and $\mathcal{M}(u)$ is the user-defined target pattern mask.

The *PD-TIA* formulation has been traditionally adopted in the state-of-the-art literature by setting uniform-sidelobe target masks [9][16] and the resulting optimization problem, often formulated as the minimization of the *mask matching error*,

$$\xi(\boldsymbol{\alpha}) \triangleq \frac{\int_{u=-1}^1 \Xi \left[\tilde{\mathcal{E}}(u; \boldsymbol{\alpha}) - \mathcal{M}(u) \right] du}{\int_{u=-1}^1 \mathcal{M}(u) du}, \quad (5)$$

$\Xi[\cdot]$ being the step function, has been addressed with several and effective strategies [9][13][16][20][21][26][27]. However, the performance of the methods formulated within the *PD* framework are generally limited by the computation of (2) for each trial solution. This may result in a non-negligible computational burden especially for large arrangements owing to the need to sample the power pattern at a sufficiently-fine angular resolution. Moreover, the *PD-TIA* formulation does not take advantage of the cyclic shift property of binary sequences [11][28], which is effectively exploited by analytical design techniques [11][16][25][28] to reduce the search space as well as to improve its sampling.

Starting from these considerations and leveraging on the theoretical framework introduced in [25], an alternative formulation of the *TIA* design problem is proposed hereinafter by reformulating the user-defined objectives from the *PD* to the *AD*. Towards this end, the power pattern expression in (2) is firstly rewritten [25] as

$$\mathcal{E}(u; \boldsymbol{\alpha}) = |F(u)|^2 \left| \sum_{k=0}^{P-1} \sqrt{\Gamma_k(\boldsymbol{\alpha})} \exp(j\psi_k(\boldsymbol{\alpha})) \times \mathcal{S} \left(\frac{2\pi\Delta zu}{\lambda} - \frac{2\pi k}{P} \right) \right|^2 \quad (6)$$

by using the *large array approximation* [2] (i.e., $F_p(u) = F(u)$, $p = 0, \dots, P-1$).

In (6), $\Gamma_k(\boldsymbol{\alpha})$ is the k -th ($k = 0, \dots, P-1$) element

$$\Gamma_k(\boldsymbol{\alpha}) \triangleq \sum_{s=0}^{P-1} \left[\gamma_s(\boldsymbol{\alpha}) \exp \left(j \frac{2\pi s}{P} k \right) \right] \quad (7)$$

of the discrete Fourier transform (*DFT*) of the *autocorrelation* of the *TIA* descriptors, $\boldsymbol{\gamma}(\boldsymbol{\alpha}) \triangleq \{\gamma_s(\boldsymbol{\alpha}); s = 0, \dots, P-1\}$, whose s -th entry is given by

$$\gamma_s(\boldsymbol{\alpha}) \triangleq \sum_{p=0}^{P-1} \alpha_p \alpha_{[p+s]_P}, \quad (8)$$

$[\cdot]_P$ being the modulo- P operator. Moreover, $\psi_k(\boldsymbol{\alpha})$ is a deterministic term equal to the phase of the k -th coefficient of the *DFT* of the descriptor sequence (i.e., $\psi_k(\boldsymbol{\alpha}) \triangleq \angle \left\{ \sum_{p=0}^{P-1} [\alpha_p \exp(j \frac{2\pi p}{P} k)] \right\}$), while $\mathcal{S}(\nu)$ is the 1D interpolation function defined as

$$\mathcal{S}(\nu) \triangleq \frac{\sin(\frac{P}{2} \times \nu)}{P \sin(\frac{\nu}{2})} \exp\left(j \frac{P-1}{2} \times \nu\right). \quad (9)$$

By sampling (6) at $u = u_k = \frac{\lambda}{P\Delta z} k$ ($k = 0, \dots, P-1$) and using the properties of the interpolation function [25], the mask-matching condition in (3) can be rewritten as follows

$$\Gamma_k(\boldsymbol{\alpha}) \leq N^2 \times \mathcal{M}\left(\frac{\lambda}{P\Delta z} k\right) \quad (10)$$

($k = 0, \dots, P-1$) since $\tilde{\mathcal{E}}(u_k; \boldsymbol{\alpha}) = \frac{\Gamma_k(\boldsymbol{\alpha})}{N^2}$ and $\mathcal{E}(0; \boldsymbol{\alpha}) = |F(u)|^2 \times N^2$ [25] ($\mathcal{E}(0; \boldsymbol{\alpha}) \triangleq |F(u)|^2 \times \left| \sum_{p=0}^{P-1} \alpha_p \right|^2$).

It is worth remarking that, even though still formulated in the *PD*, (10) highlights the relationship between the *DFT* of the autocorrelation of $\boldsymbol{\alpha}$ (on the left-hand) and the user-defined mask requirements (on the right-hand). To formulate the *TIA* synthesis in the *AD*, it would be in principle easy to apply the inverse *DFT* (*IDFT*) operator directly to (10), but this is not possible since the Fourier Transform is not a monotonic operator and it cannot be applied to inequalities such as that in (10). To circumvent such an issue, the solution domain is bounded to the descriptors $\boldsymbol{\alpha}$ that fulfil the *equality-restricted* version of (10):

$$\Gamma_k(\boldsymbol{\alpha}) = N^2 \times \mathcal{M}\left(\frac{\lambda}{P\Delta z} k\right) \quad (11)$$

($k = 0, \dots, P-1$). Thanks to this assumption, the *TIA* design problem can be formulated in the *AD* as follows

Mask-Equality Autocorrelation-Domain TIA (ME-AD-TIA) Design Problem - Find $\boldsymbol{\alpha}^{opt}$ [$\boldsymbol{\alpha}^{opt} \in \mathcal{D}(\boldsymbol{\alpha})$] such that the condition

$$\gamma_s(\boldsymbol{\alpha}^{opt}) = N^2 \times \mu_s(\mathbf{M}) \quad (12)$$

$(s = 0, \dots, P - 1)$ is fulfilled, $\mathbf{M} \triangleq \left\{ M_k \triangleq \mathcal{M} \left(\frac{\lambda}{P\Delta z} k \right); k = 0, \dots, P - 1 \right\}$ being the set of P mask samples, while

$$\mu_s(\mathbf{M}) \triangleq \frac{1}{P} \sum_{k=0}^{P-1} \left[M_k \exp \left(-j \frac{2\pi k}{P} s \right) \right] \quad (13)$$

is the corresponding s -th ($s = 0, \dots, P - 1$) *IDFT* coefficient.

Unfortunately this *AD* formulation has some drawbacks since strictly enforcing (12) is not actually equivalent to fulfill (10). First of all, such a reformulation may result in a physically unfeasible problem. As a matter of fact, there is no guarantee that there is a *TIA* that radiates a pattern matching an - even though realistic - arbitrary user-defined mask $\mathcal{M}(u)$ in a discrete, but uniform, set of angular points. Otherwise, sub-optimal *TIA* layouts may be synthesized owing to the over-constrained nature of the design problem at hand.

Therefore, an alternative *AD*-based approach is introduced. More specifically, instead of directly fulfilling the mask constraints, the *TIA* descriptors are set to match the autocorrelation function of an *auxiliary* fully-populated array (*AFPA*) with excitations $\mathbf{w}^{feas} \triangleq \{w_p^{feas}; p = 0, \dots, P - 1\}$ whose pattern complies with the user-defined (realistic) mask $\mathcal{M}(u)$:

$$\mathbf{w}^{feas} = \arg \left\{ \max_{\mathbf{w}} [\mathcal{E}(0; \mathbf{w})] \mid \mathcal{E}(u; \mathbf{w}) \leq \mathcal{M}(u) \right\}. \quad (14)$$

This problem is now always feasible, the target autocorrelation being that of a fully-populated array fulfilling (3). Moreover, since (14) is a constrained convex minimization problem, it can be solved by conventional deterministic techniques [1][29][30].

Mathematically, the arising *TIA* synthesis problem can be then stated as

Feasible-Pattern-Equality Autocorrelation-Domain TIA (FPE-AD-TIA) Design Problem - Find $\boldsymbol{\alpha}^{opt}$ [$\boldsymbol{\alpha}^{opt} \in \mathcal{D}(\boldsymbol{\alpha})$] such that

$$\gamma_s(\boldsymbol{\alpha}^{opt}) = N^2 \times \mu_s(\mathbf{E}^{feas}) \quad (15)$$

$(s = 0, \dots, P - 1)$ holds true.

In (15), \mathbf{E}^{feas} consists of the samples of the auxiliary pattern $\mathcal{E}^{feas}(u)$ [$\mathcal{E}^{feas}(u) \triangleq \mathcal{E}(u; \mathbf{w}^{feas})$]

$$\mathbf{E}^{feas} \triangleq \left\{ E_k^{feas} \triangleq \mathcal{E}^{feas} \left(\frac{\lambda}{P\Delta z} k \right); k = 0, \dots, P-1 \right\} \quad (16)$$

and the s -th ($s = 0, \dots, P-1$) *feasible autocorrelation* coefficient, $\mu_s(\mathbf{E}^{feas})$, is equal to

$$\mu_s(\mathbf{E}^{feas}) \triangleq \frac{1}{P} \sum_{k=0}^{P-1} \left[\mathcal{E}^{feas} \left(\frac{\lambda}{P\Delta z} k \right) \exp \left(-j \frac{2\pi k}{P} s \right) \right]. \quad (17)$$

Unlike the *ME-AD-TIA* formulation, the *FPE-AD-TIA* one yields to a two-step solution process where (i) an *AFPA* is firstly derived by solving (14) through a state-of-the-art convex programming technique [1][29] and (ii) the actual *TIA* design step is carried out afterwards in the *AD* according to (15). Since several efficient algorithms are available to address the auxiliary step (i), including the popular Matlab subroutine *fmincon* [1][29][30], only the step (ii) with the solution of (15) will be detailed in the following.

It is worthwhile to point out that the conceived autocorrelation-driven paradigm is not limited to the constraints stated in (12) or (15), but alternative objectives may be seamlessly taken into account within the same framework by exploiting (17), thus defining an *AFPA* that fulfils (even) non pattern-related constraints (e.g., capacity maximization).

3 Evolutionary-Based *TIA* Synthesis

The solution of the *TIA* synthesis problem, α^{opt} [$\alpha^{opt} \in \mathcal{D}(\alpha)$], in the *AD* for both the *ME-AD-TIA* (12) and the *FPE-AD-TIA* (15) formulations (analogously to that in the *PD*) requires a suitable search procedure to efficiently/effectively sample the solution space $\mathcal{D}(\alpha)$. Indeed, (a) the relation between the *DoFs* of the *TIA* design, α , and the corresponding synthesis objective is highly non-linear by definition of the autocorrelation function (8), and (b) both the dimensionality and the cardinality of $\mathcal{D}(\alpha)$ of a realistic *TIA* design problem may be very huge, P being in the order of hundreds. Moreover, (c) the binary nature of the unknowns suggests to consider a binary-variable global optimizer as solver tool [24].

However, just addressing the problem solution as a standard binary optimization may be sub-

optimal since it would neglect some analytic properties of the autocorrelation function (8). For instance, it is known from combinatorial theory [11][25] that a σ -positions cyclically-shifted version of any *parent* sequence α , $\alpha^{(\sigma)}$, which is defined as

$$\alpha^{(\sigma)} \triangleq \{\alpha_{\lfloor p+\sigma \rfloor_P}; p = 0, \dots, P-1\}, \quad (18)$$

exhibits the same autocorrelation function of the generating sequence (*invariance property*), that is

$$\gamma_s(\alpha^{(\sigma)}) \equiv \gamma_s(\alpha) \quad (19)$$

($s = 0, \dots, P-1$). The exploitation of such a property (19) in the *AD* problem formulations can play a significant role in efficiently sampling $\mathcal{D}(\alpha)$ towards α^{opt} . As a matter of fact and unlike conventional *PD*-based strategies, the size of $\mathcal{D}(\alpha)$ can be considerably “shrunked” by taking into account that the set of cyclically-shifted versions of a parent sequence (i.e., $\{\alpha^{(\sigma)}; \sigma = 0, \dots, P-1\}$) has the same autocorrelation function.

Accordingly, the global binary optimizer adopted for solving the *AD*-based *TIA* problems is only responsible of generating the *parent* sequences, while the actual optimal α^{opt} is afterwards found by simply comparing the members of the selected α -family [i.e., directly checking the P shifted sequences generated with (18)]. In particular, a genetic algorithm (*GA*)-based mechanism [9][16][17][24] is used to evolve the parents sequences owing to (a) its well-known effectiveness in solving discrete problems with highly non-linear and multi-minima cost functions to be minimized/maximized [24], (b) the excellent results in dealing with standard *TIA* syntheses [9][16][17], and (c) the possibility to easily include *a-priori* knowledge and/or design constraints by suitably adjusting the evolutionary operators [16][17]. More in detail, the proposed *GA*-based technique implements the following customizations with respect to the state-of-the-art *GAs* [9][16][17]:

- **Initialization** ($i = 0$) - As for the *ME-AD-TIA* formulation, use a standard random initialization by setting the q -th ($q = 0, \dots, Q-1$; Q being the population size) trial solution $\alpha^{(q)}$ to

$$\alpha_0^{(q)} \triangleq \{\alpha_{p0}^{(q)} = r_p^{(q)}; p = 0, \dots, P-1\}, \quad (20)$$

$r_p^{(q)}$ being a random binary digit, while exploit the auxiliary excitation set \mathbf{w}^{feas} for the *FPE-AD-TIA* implementation as follows

$$\boldsymbol{\alpha}_0^{(q)} \triangleq \left\{ \alpha_{p0}^{(q)} = \mathcal{R} \left[w_{[p+q]_P}^{feas} \right]; p = 0, \dots, P-1 \right\} \quad (21)$$

($q = 0, \dots, Q-1$) $\mathcal{R}[\cdot]$ being the rounding operator (i.e., $\mathcal{R}[\cdot] = 1$ if $[\cdot] \geq 0.5$, $\mathcal{R}[\cdot] = 0$ otherwise);

- **Cost Function** - Define the cost function, which quantifies the $\boldsymbol{\alpha}$ -solution optimality, as

$$\Phi(\boldsymbol{\alpha}) \triangleq \frac{\sum_{s=0}^{P-1} |\gamma_s(\boldsymbol{\alpha}) - \gamma_s^*|^2}{P} \quad (22)$$

by setting γ_s^* ($s = 0, \dots, P-1$) to $\gamma_s^* = N^2 \times \mu_s(\mathbf{M})$ and $\gamma_s^* = N^2 \times \mu_s(\mathbf{E}^{feas})$ for the *ME-AD-TIA* formulation and the *FPE-AD-TIA* one, respectively;

- **GA Termination** - Stop the iterative process of generating the i -th ($i = 1, \dots, I$; I being the maximum number of iterations) population of trial solutions, $\{\boldsymbol{\alpha}_i^{(q)}; q = 0, \dots, Q-1\}$, when either $i = I$ ($\rightarrow i_{conv} = I$) or the following *stagnation condition*

$$\left| \Phi_i^{best} - \frac{1}{L} \sum_{i=l-L}^{l-1} \Phi_i^{best} \right| \leq \Phi_{th} \quad (23)$$

holds true ($\rightarrow i_{conv} = i$). In (23), Φ_{th} is the user-defined convergence threshold, Φ_i^{best} is the cost function value of the best guess found until the i -th ($i = 1, \dots, I$) iteration, and L is the length of the stagnation window. Deduce the optimal *parent* sequence $\hat{\boldsymbol{\alpha}}$ as $\hat{\boldsymbol{\alpha}} = \arg \{ \min_{q=0, \dots, Q-1} \min_{i=0, \dots, I-1} [\Phi(\boldsymbol{\alpha}_i^{(q)})] \}$;

- **Post-GA Cyclic Shift** - Output the final *TIA* layout, $\boldsymbol{\alpha}^{opt}$, by applying the cyclic σ -shift procedure to the optimal parent sequence $\hat{\boldsymbol{\alpha}}$ and select that one with the minimum value of the mask matching error $\xi(\hat{\boldsymbol{\alpha}}^{(\sigma)})$

$$\boldsymbol{\alpha}^{opt} \triangleq \arg \left\{ \min_{\sigma=0, \dots, P-1} [\xi(\hat{\boldsymbol{\alpha}}^{(\sigma)})] \right\}. \quad (24)$$

For the sake of completeness, the flowchart of this *GA*-based design process is reported in Fig. 1(b) where the non-standard operators have been highlighted with a red contour.

Concerning the computational complexity, it is worth noticing that (a) the cost function in (22) is evaluated in the *AD* and not in the *PD* as (3) with an inexpensive operation without requiring a (fine) sampling of the power pattern, (b) the local search, implemented throughout the “*Post-GA Cyclic Shift*”, actually requires (24) the computation of the normalized pattern $\tilde{\mathcal{E}}(u; \hat{\alpha}^{(\sigma)})$ (4) and the evaluation of its deviation from the mask $\mathcal{M}(u)$ (5) only for P shifted sequences.

4 Numerical Assessment and Validation

This section is devoted to assess the proposed *AD*-based thinning approach and its algorithmic implementations as well as to derive suitable guidelines for its application. Moreover, the results from comparisons with conventional *PD*-based methods will be reported to point out the effectiveness and the efficiency of the *AD*-driven synthesis paradigm.

The first numerical analysis is aimed at illustrating the features of the *AD* formulation in comparison with the traditional *PD* one. Towards this end, a half-wavelength spaced ($\Delta z = \frac{\lambda}{2}$) *TIA* composed of $P = 16$ ideal radiators and complying with the following mask

$$\mathcal{M}(u) = \begin{cases} 0 \text{ [dB];} & -\frac{1.0}{P} < u < \frac{1.0}{P} \\ -15 \text{ [dB];} & \textit{otherwise} \end{cases} \quad (25)$$

has been chosen as benchmark so that it has been possible to *exhaustively* compute both the *PD* (5) and the *AD* (22) cost functions thanks to the limited size (i.e., $H = 2^P$) of the solution space of the whole set of admissible thinning sequences ($\mathcal{D}(\alpha) = \{\alpha_h; h = 1, \dots, H\}$).

Figure 2 shows the relative frequency of the cost function values for both *PD* [Fig. 2(a) - $\xi(\alpha)$] and *AD* [Fig. 2(b) - $\Phi(\alpha)$] formulations. From the inset of Fig. 2(a), one can notice that there are several sub-optimal solutions in close proximity to the optimal one (i.e., $\alpha^{opt} = \arg\{\xi(\alpha) = 0\}$) in the *PD* case. This outcome points out the complexity of identifying the actual global optimum α^{opt} when adopting the *PD* formulation, regardless of the solution method. On the contrary, the occurrence of sub-optimal solutions near to α^{opt} ($\alpha^{opt} = \arg\{\Phi(\alpha) = 0\}$) [see the inset of Fig. 2(b)] significantly reduces in the *AD* formu-

lation, thus avoiding “local minima” for finding the global one turns out to be an easier task.

In the following, the numerical analysis will be devoted to assess the effectiveness of the iterative approach discussed in Sect. 3 to faithfully and efficiently retrieve the global optimum *TIA* layout. Within this framework, the first test case is concerned with the synthesis of a $P = 24$ *TIA*, the target autocorrelation γ^* ($\gamma^* \triangleq \{\gamma_s^*; s = 0, \dots, P - 1\}$) being the known three-level function coming from an Almost Difference Set (*ADS*) sequence α^{ADS} [11][12]. Such a choice has been done since identifying binary sequences complying with the unique properties of *ADS*s is usually a complex task even for small apertures [16].

Figure 3 summarizes the results. More specifically, Figure 3(a) shows that the autocorrelation function of the best parent $\hat{\alpha}$ is equal, as expected, to that of the final design α^{opt} and they coincide with the target one, α^{ADS} , by proving the effectiveness of the synthesis strategy to explore the autocorrelation solution space and to identify the global optimum despite the wide dimensionality ($H = 2^{24}$) of search space $\mathcal{D}(\alpha)$. Moreover, the plot of the convergence values of the cost function (22) for $V = 100$ different runs of the evolutionary strategy, $\{\Phi_{i_{conv}}^{best} |_{v}; v = 1, \dots, V\}$, in Fig. 3(b) assesses the robustness of the stochastic solver since only in few v -th cases $\Phi_{i_{conv}}^{best} |_{v} \neq 0$, the value $\Phi_{i_{conv}}^{best} = 0$ being that of a parent sequence $\hat{\alpha}$ with an autocorrelation function equal to the target one. Figure 3(b) also reports the Hamming distance between α^{ADS} and $\hat{\alpha}$,

$$\rho(\hat{\alpha}, \alpha^{ADS}) \triangleq \sum_{p=0}^{P-1} \frac{|\hat{\alpha}_p - \alpha_p^{ADS}|}{\alpha_p^{ADS}}, \quad (26)$$

to highlight that generally the *TIA* sequence found at the “*GA Termination*” step, $\hat{\alpha}$, is not equal to α^{ADS} , but one of its cyclic shifted versions since $\rho(\hat{\alpha}, \alpha^{ADS}) > 0$. Such a result points out a key feature of the *AD* formulation, that is the reduction of the search space, since the whole set of shifted versions of a binary thinning sequence shares the same value of (22). For instance, the parent sequence $\hat{\alpha}$ in Fig. 3(c) is quite different from α^{ADS} in Fig. 3(d), but $\Phi(\hat{\alpha}) = \Phi(\alpha^{ADS})$. On the other hand, afterwards it is mandatory to apply the “*Post-GA Cyclic Shift*” to identify, through simple comparisons (24), the best shifted version of the parent sequence $\hat{\alpha}$ (i.e., α^{opt}) that turns out to be equal to α^{ADS} .

In the the next example, the target autocorrelation function is not *a-priori* known and the *TIA* synthesis is formulated in terms of pattern-mask constraints, $\mathcal{M}(u)$. More specifically, such

an experiment is aimed at illustrating the step-by-step application of the *ME-AD-TIA* approach when dealing with the $P = 24$ layout fulfilling the constant sidelobe pattern (25) (Fig. 4). Since the method forces the exact match with the target mask $\mathcal{M}(u)$ in the sampling points [i.e., $\mathcal{E}^{ME}(\frac{\lambda}{P\Delta z}k) = M_k$; $k = 0, \dots, P - 1$ being $\mathcal{E}^{ME}(u) \triangleq \mathcal{E}(u; \alpha_{ME}^{opt})$] [Fig. 4(a)], the target autocorrelation γ_{ME}^* [e.g., here the two-level envelope in Fig. 4(b)] could be a non-feasible function as confirmed by the behavior of the cost function (22) vs. the iteration index in Fig. 5(a). Indeed, the synthesis process does not reach the condition $\Phi_{i_{conv}}^{best} = 0$. However, the autocorrelation of $\hat{\alpha}^{ME}$, $\hat{\gamma}^{ME}$ [$\hat{\gamma} \triangleq \gamma(\hat{\alpha})$], and the target one, γ_{ME}^* , turn out to be very close [see yellow vs. red plots in Fig. 5(b)]. Of course, the same holds true for all the cyclically-shifted sequences, $\{\hat{\alpha}^{(\sigma)}; \sigma = 0, \dots, P - 1\}$, generated by the parent sequence $\hat{\alpha}^{ME}$ [Fig. 6(a)], which include the optimal one α_{ME}^{opt} [Fig. 6(b)] having the minimum value of (5) [Fig. 5(c)] according to (24).

The comparison among the target pattern-mask $\mathcal{M}(u)$ and the patterns from $\hat{\alpha}^{ME}$ and α_{ME}^{opt} in Fig. 6(c) highlights several key features of the *ME-AD-TIA* implementation: (i) enforcing a “strict” matching with $\mathcal{M}(u)$ may yield to an ‘unfeasible’ synthesis problem [Fig. 6(c)]; (ii) the sidelobes of the synthesized pattern, $\mathcal{E}^{ME}(u)$, may exceed the mask, $\mathcal{M}(u)$ [i.e., $\mathcal{E}^{ME}(u) > \mathcal{M}(u)$] since the matching is enforced at the sampling points $\{u_k = \frac{\lambda}{P\Delta z}k; k = 0, \dots, P - 1\}$ [Fig. 6(c)]; (iii) despite its simplicity, the “*Post-GA Cyclic Shift*” significantly improves the *SLL* of the synthesized solution [i.e., $SLL^{ME} = -10.92$ [dB] ($SLL^{ME} \triangleq SLL\{\mathcal{E}^{ME}(u)\}$) vs. $\widehat{SLL}^{ME} = -6.85$ [dB] ($\widehat{SLL}^{ME} \triangleq SLL\{\hat{\mathcal{E}}^{ME}(u)\}$); $\hat{\mathcal{E}}^{ME}(u) \triangleq \mathcal{E}(u; \hat{\alpha}^{ME})$] - Fig. 6(c)].

It is worth pointing out that, also in this example of a wider aperture [i.e., $P = 24$ vs. $P = 16$], one can still infer the same outcomes on the distribution of the local minima drawn from Fig. 2. Once more, the *AD* formulation turns out to be more suitable for the synthesis of an optimal *TIA* [i.e., Fig. 7(b) vs. Fig. 7(a)].

The same benchmark scenario has then be treated with the *FPE-AD-TIA* method. Therefore, the feasible auxiliary excitation set \mathbf{w}^{feas} has been computed by solving the corresponding conventional mask-constrained fully-populated array design problem [1][29][30] with the Matlab subroutine *fmincon* [1][29][30]. The plots of $\mathcal{E}^{feas}(u)$ and the corresponding samples, $\{E_k^{feas}; k = 0, \dots, P - 1\}$, show that, unlike the *ME* approach, the *FPE* implementation does not require

the target pattern values to be equal to the mask ones [i.e., $E_k^{feas} \leq M_k, k = 0, \dots, P - 1$ - Fig. 4(a) and Fig. 8(d)]. Consequently, the target autocorrelation γ_{FPE}^* turns out to be different from that of the *ME* case γ_{ME}^* [Fig. 4(b)] even though, also in the *FPE* case, $\hat{\gamma}^{FPE} \neq \gamma_{FPE}^*$ [Fig. 8(a)] such as $\hat{\gamma}^{ME} \neq \gamma_{ME}^*$ [Fig. 5(b)]. The result is that the *FPE* pattern $\mathcal{E}^{FPE}(u)$ [Fig. 8(d)] better complies with the pattern mask [Fig. 8(d) vs. Fig. 6(c)]. In particular, the *SLL* of the *FPE* layout α_{FPE}^{opt} in Fig. 8(c) is smaller than the *ME* one [i.e., $SLL^{FPE} - SLL^{ME} = -3.54$ [dB] - Fig. 8(d) vs. Fig. 6(c)] and the mask $\mathcal{M}(u)$ is violated only in a few angular samples [Fig. 8(d)]. As theoretically expected, the *FPE* implementation guarantees, on the one hand, an efficient solution space exploration thanks to the *AD* formulation, and on the other hand, an intrinsically more accurate pattern control than the *ME* technique.

The dependence of the performance of the *AD-TIA* strategies on the *SLL* of the target pattern mask is analyzed next by still considering the previous $P = 24$ elements benchmark array. The behavior of $\xi(\alpha^{opt})$ [$\xi_{opt} \triangleq \xi(\alpha^{opt})$] versus the *SLL* value (Fig. 9) in (25) confirms the enhancement of the pattern control enabled by the *FPE* implementation. As theoretically expected, owing to the limited aperture ($P = 24$) and the binary nature of the *TIA*, the advantage of adopting the *FPE-AD* method reduces more and more as the *SLL* constraint gets harder and harder (e.g., $\xi_{opt}^{FPE} \Big|_{SLL=-15[\text{dB}]} = 2.06 \times 10^{-4}$ vs. $\xi_{opt}^{ME} \Big|_{SLL=-15[\text{dB}]} = 7.38 \times 10^{-3}$; $\xi_{opt}^{FPE} \Big|_{SLL=-30[\text{dB}]} = 1.95 \times 10^{-2}$ vs. $\xi_{opt}^{ME} \Big|_{SLL=-30[\text{dB}]} = 2.35 \times 10^{-2}$ - Fig. 9) until unfeasible for the array at hand.

The fifth test case is concerned with more complex pattern masks, namely the ‘‘Tapered Mask’’ (*TM*) [Fig. 10(a)] and the ‘‘Irregular Mask’’ (*IM*) [Fig. 10(b)]. The *TIA* layouts synthesized with the *FPE-AD* [Figs. 10(a)-10(b)] turn out to be almost completely compliant with the corresponding pattern masks $\mathcal{M}(u)$ [Figs. 10(c)-10(d)]. Moreover, once again the ‘‘*Post-GA Cyclic Shift*’’ significantly improves the mask fitting of the parent sequence $\hat{\mathcal{E}}^{FPE}(u)$ since $\xi_{opt}^{FPE} < \hat{\xi}^{FPE}$ [$\hat{\xi} \triangleq \xi(\hat{\alpha})$]: $\xi_{opt}^{FPE} \Big|_{TM} = 1.78 \times 10^{-4}$ vs. $\hat{\xi}^{FPE} \Big|_{TM} = 2.57 \times 10^{-3}$ and $\xi_{opt}^{FPE} \Big|_{IM} = 9.86 \times 10^{-4}$ vs. $\hat{\xi}^{FPE} \Big|_{IM} = 1.52 \times 10^{-2}$.

To assess the reliability of the *AD*-based *TIA* synthesis in real systems where coupling effects arise along with other non-idealities, the design of an array composed of cavity-backed slot-fed patch antennas that resonate at 28 GHz [see Fig. 11(a) and Tab. I] to afford the element pattern

in Fig. 11(b) has been carried out by enforcing the same mask profiles of Fig. 10. Figure 12 shows the plots of the 3D [Figs. 12(a)-12(b)] and the 2D [Figs. 12(c)-12(d)] full-wave *HFSS* simulated patterns of the *FPE* optimized layouts. The comparisons between ideal and *HFSS* full-wave simulated patterns in the elevation cut [Figs. 12(c)-12(d)], the pattern mask $\mathcal{M}(u)$ being also reported, point out the robustness of the synthesis method, the values of the mask matching error for the *HFSS* models being very close to the ideal ones [i.e., $\xi_{opt}^{FPE}]_{TM}^{Ideal} = 1.78 \times 10^{-4}$ vs. $\xi_{opt}^{FPE}]_{TM}^{HFSS} = 9.42 \times 10^{-5}$ - Fig. 12(c); $\xi_{opt}^{FPE}]_{IM}^{Ideal} = 9.86 \times 10^{-4}$ vs. $\xi_{opt}^{FPE}]_{IM}^{HFSS} = 8.71 \times 10^{-4}$ - Fig. 12(d)].

The last experiment compares the *FPE-AD* approach with a traditional *PD*-based one for different apertures. More specifically, the number of array elements has been varied from $P = 16$ up to $P = 128$, while enforcing the pattern mask $\mathcal{M}(u)$ in Fig. 13(d) [“Irregular Mask [Type 2]” (*IM2*)] and setting the width of the main beam to $\frac{2}{P}$. The plot of the values of the matching error ξ versus P are shown in Fig. 13(a). As it can be clearly inferred, the *AD*-based method overcomes the *PD* one regardless of the array aperture since always $\xi_{opt}^{FPE-AD} < \xi_{opt}^{PD}$ [Fig. 13(a)]. For illustrative purposes, Figure 13(d) reports the power patterns radiated by the $P = 48$ array layouts in Figs. 13(b)-13(c). In this case, $\xi_{opt}^{FPE-AD}]_{P=48} = 1.47 \times 10^{-3}$, while $\xi_{opt}^{PD}]_{P=48} = 8.97 \times 10^{-3}$ [Fig. 13(a)].

As for the computational cost, the plots of the synthesis time, Δt , versus the array size P are given in Fig. 14(a). It is worthwhile to point out that non-optimized *MATLAB* implementations have been considered for both *AD*- and *PD*-based formulations, the SW codes being executed on single-core laptop with 2.4 [GHz] *CPU*. As expected and claimed at the bottom of Sect. 3, thanks to the faster cost function computation (22) in the solution-search process, the *AD* synthesis turns out to be considerably more efficient regardless of the *TIA* aperture (i.e., $-97.2\% \leq \frac{\Delta t^{FPE-AD} - \Delta t^{PD}}{\Delta t^{PD}} \leq -93.1\%$ - Fig. 14).

5 Conclusions and Final Remarks

An innovative *TIA* synthesis method leveraging on the theoretical framework developed in [25] has been proposed. Unlike traditional *PD*-formulated approaches, the *TIA* design process has been recast as the problem of matching a target autocorrelation function derived from the user-

defined guidelines and synthesis-objectives modeled as a pattern mask. Two different implementations of the *AD*-based formulation of the *TIA* synthesis problem have been proposed and a binary hybrid optimization approach has been detailed.

The numerical validation has shown that

- formulating the *TIA* synthesis problem in the *AD*, instead of the *PD*, reduces the complexity of the solution process;
- unlike [25], arbitrary mask constraints can be handled (Fig. 10);
- within the *AD* problem formulation, the *FPE* implementation performs better than the *ME* one in terms of both target-mask fulfillment (Fig. 9) and control of the peak sidelobes (Fig. 6 vs. Fig 8);
- the proposed *TIA* synthesis is robust to mutual coupling effects (Fig. 12);
- thanks to the reduction of the local minima, the “shrinking” of the solution space, and the faster cost function computation [(22) vs. (5)], *AD*-based design methods are much more computationally-efficient than the state-of-the-art *PD* alternatives (Fig. 14).

Future works, beyond the scope of this paper, will be aimed at either extending to other classes of unconventional/conventional arrays beyond *TIA* (e.g., clustered, overlapped, thinned as well as fully-populated arrangements) the proposed *AD*-based design method, owing to the generality of the *AD* theory, or handling various kinds of constraints also different from the pattern mask ones. Moreover, the design of planar as well as conformal layouts will be the subject of future works.

Acknowledgements

This work benefited from the networking activities carried out in the Project “ICSC National Centre for HPC, Big Data and Quantum Computing (CN HPC)” funded by the European Union - NextGenerationEU within the PNRR Program (CUP: E63C22000970007), the Project

“INSIDE-NEXT - Indoor Smart Illuminator for Device Energization and Next-Generation Communications” Funded by the European Union under NextGenerationEU (CUP: E53D23000990001), the Project “AURORA - Smart Materials for Ubiquitous Energy Harvesting, Storage, and Delivery in Next Generation Sustainable Environments” funded by the Italian Ministry for Universities and Research within the PRIN-PNRR 2022 Program (CUP: E53D23014760001), the Project “Telecommunications of the Future” (PE00000001 - program “RESTART”, Structural Project 6GWINET) funded by European Union under the Italian National Recovery and Resilience Plan (NRRP) of NextGenerationEU (CUP: D43C22003080001), the Project "Telecommunications of the Future" (PE00000001 - program “RESTART”, Focused Project MOSS) funded by European Union under the Italian National Recovery and Resilience Plan (NRRP) of NextGenerationEU (CUP: J33C22002880001), the Project “Telecommunications of the Future” (PE00000001 - program “RESTART”, Structural Project IN) funded by European Union under the Italian National Recovery and Resilience Plan (NRRP) of NextGenerationEU (CUP: J33C22002880001), the Project “Smart ElectroMagnetic Environment in TrentiNo - SEME@TN” funded by the Autonomous Province of Trento (CUP: C63C22000720003), and the Project DICAM-EXC (Grant L232/2016) funded by the Italian Ministry of Education, Universities and Research (MUR) within the “Departments of Excellence 2023-2027” Program (CUP: E63C22003880001).

A. Massa wishes to thank E. Vico for her never-ending inspiration, support, guidance, and help.

References

- [1] P. Rocca, G. Oliveri, R. J. Mailloux, and A. Massa, “Unconventional phased array architectures and design methodologies - A review," *Proc. IEEE*, vol. 104, no. 3, pp. 544-560, Mar. 2016.
- [2] R. J. Mailloux, *Phased Array Antenna Handbook*, 2nd ed. Norwood, MA, USA: Artech House, 2005.
- [3] R. L. Haupt, *Antenna Arrays - A Computation Approach*. Hoboken, NJ, USA: Wiley, 2010.

- [4] G. Oliveri, G. Gottardi, F. Robol, A. Polo, L. Poli, M. Salucci, M. Chuan, C. Massagrande, P. Vinetti, M. Mattivi, R. Lombardi, and A. Massa, "Co-design of unconventional array architectures and antenna elements for 5G base stations," *IEEE Trans. Antennas Propag.*, vol. 65, no. 12, pp. 6752-6766, Dec. 2017.
- [5] N. Anselmi, P. Rocca, S. Feuchtinger, B. Biscontin, A. M. Barrera, and A. Massa, "Optimal capacity-driven design of aperiodic clustered phased arrays for multi-user MIMO communication systems," *IEEE Trans. Antennas Propag.*, vol. 70, no. 7, pp. 5491-5505, Jul. 2022.
- [6] C. Cui, W. T. Li, X. T. Ye, Y. Q. Hei, P. Rocca, and X. W. Shi, "Synthesis of mask-constrained pattern-reconfigurable nonuniformly spaced linear arrays using Artificial Neural Networks," *IEEE Trans. Antennas Propag.*, vol. 70, no. 6, pp. 4355-4368, Jun. 2022.
- [7] P. Rocca, L. Poli, N. Anselmi, and A. Massa, "Nested optimization for the synthesis of asymmetric shaped beam patterns in subarrayed linear antenna arrays," *IEEE Trans. Antennas Propag.*, vol. 70, no. 5, pp. 3385-3397, May 2022.
- [8] M. Skolnik, J. W. Sherman, and F. C. Ogg, "Statistically designed density-tapered arrays," *IEEE Trans. Antennas Propag.*, vol. 12, no. 4, pp. 408-417, Jul. 1964.
- [9] R. L. Haupt, "Thinned arrays using genetic algorithms," *IEEE Trans. Antennas Propag.*, vol. 42, no. 7, pp. 993-999, Jul. 1994.
- [10] M. G. Bray, D. H. Werner, D. W. Boeringer, and D. W. Machuga, "Optimization of thinned aperiodic linear phased arrays using genetic algorithms to reduce grating lobes during scanning," *IEEE Trans. Antennas Propag.*, vol. 50, no. 12, pp. 1732-1742, Dec. 2002.
- [11] G. Oliveri, M. Donelli, and A. Massa, "Linear array thinning exploiting almost difference sets," *IEEE Trans. Antennas Propag.*, vol. 57, no. 12, pp. 3800-3812, Dec. 2009.
- [12] G. Oliveri, L. Manica, and A. Massa, "ADS-Based guidelines for thinned planar arrays," *IEEE Trans. Antennas Propag.*, vol. 58, no. 6, pp. 1935-1948, Jun. 2010.

- [13] W. P. M. N. Keizer, "Linear array thinning using iterative FFT techniques," *IEEE Trans. Antennas Propag.*, vol. 56, no. 8 (II), pp. 2757-2760, 2008.
- [14] G. Oliveri and A. Massa, "Fully-interleaved linear arrays with predictable sidelobes based on almost difference sets," *IET Radar, Sonar Navig.*, vol. 4, no. 5, pp. 649-661, 2010.
- [15] G. Oliveri, F. Viani, and A. Massa, "Synthesis of linear multi-beam arrays through hierarchical ADS-based interleaving," *IET Microw. Antennas Propag.*, vol. 8, no. 10, pp. 794-808, Jul. 2014.
- [16] G. Oliveri and A. Massa, "GA-enhanced ADS-based approach for array thinning," *IET Microw. Antennas Propag.*, vol. 5, no. 3, pp. 305-315, 2011.
- [17] M. Salucci, G. Gottardi, N. Anselmi, and G. Oliveri, "Planar thinned array design by hybrid analytical-stochastic optimization," *IET Microw. Antennas Propag.*, vol. 11, no. 13, pp. 1841-1845, Oct. 2017.
- [18] D. H. Wolpert and W. G. Macready, "No free lunch theorems for optimization," *IEEE Trans. Evol. Comput.*, vol. 1, no. 1, pp. 67-82, Apr. 1997.
- [19] R. J. Mailloux and E. Cohen, "Statistically thinned arrays with quantized element weights," *IEEE Trans. Antennas Propag.*, vol. 39, no. 4, pp. 436-447, Apr. 1991.
- [20] O. Quevedo-Teruel and E. Rajo-Iglesias, "Ant colony optimization in thinned array synthesis with minimum sidelobe level," *IEEE Antennas Wireless Propag. Lett.*, vol. 5, no. 1, pp. 349-352, 2006.
- [21] K. V. Deligkaris, Z. D. Zaharis, D. G. Kampitaki, S. K. Goudos, I. T. Rekanos, and M. N. Spasos, "Thinned planar array design using boolean PSO with velocity mutation," *IEEE Trans. Magn.*, vol. 45, no. 3, pp. 1490-1493, Mar. 2009.
- [22] K. Guney and M. Onay, "Synthesis of thinned linear antenna arrays using bees algorithm," *Microw. Opt. Technol. Lett.*, vol. 53, no. 4, pp. 795-799, Apr. 2011.

- [23] B. Ha, M. Mussetta, P. Pirinoli, and R. E. Zich, "Modified compact genetic algorithm for thinned array synthesis," *IEEE Antennas Wireless Propag. Lett.*, vol. 15, pp. 1105-1108, 2016.
- [24] P. Rocca, M. Benedetti, M. Donelli, D. Franceschini, and A. Massa, "Evolutionary optimization as applied to inverse problems," *Inverse Probl.*, vol. 25, pp. 1-41, Dec. 2009.
- [25] G. Oliveri, G. Gottardi, M. A. Hannan, N. Anselmi, and L. Poli, "Autocorrelation-driven synthesis of antenna arrays - The case of DS-based planar isophoric thinned arrays," *IEEE Trans. Antennas Propag.*, vol. 68, no. 4, pp. 2895-2910, Apr. 2020.
- [26] L. Gu, Y. -W. Zhao, Z. -P. Zhang, L. -F. Wu, Q. -M. Cai, and J. Hu, "Linear array thinning using probability density tapering approach," *IEEE Antennas Wireless Propag. Lett.*, vol. 18, no. 9, pp. 1936-1940, Sep. 2019.
- [27] X. Wang, E. Aboutanios, and M. G. Amin, "Thinned array beam pattern synthesis by iterative soft-thresholding-based optimization algorithms," *IEEE Trans. Antennas Propag.*, vol. 62, no. 12, pp. 6102-6113, Dec. 2014.
- [28] D. G. Leeper, "Isophoric arrays - Massively thinned phased arrays with well-controlled sidelobes," *IEEE Trans. Antennas Propag.*, vol. 47, no. 12, pp. 1825-1835, 1999.
- [29] D. Sartori, G. Oliveri, L. Manica, and A. Massa, "Hybrid design of non-regular linear arrays with accurate control of the pattern sidelobe," *IEEE Trans. Antennas Propag.*, vol. 61, no. 12, pp. 6237-6242, Dec. 2013.
- [30] M. D. Urso and T. Isernia, "Solving some array synthesis problems by means of an effective hybrid approach," *IEEE Trans. Antennas Propag.*, vol. 55, no. 3, pp. 750-759, Mar. 2007.

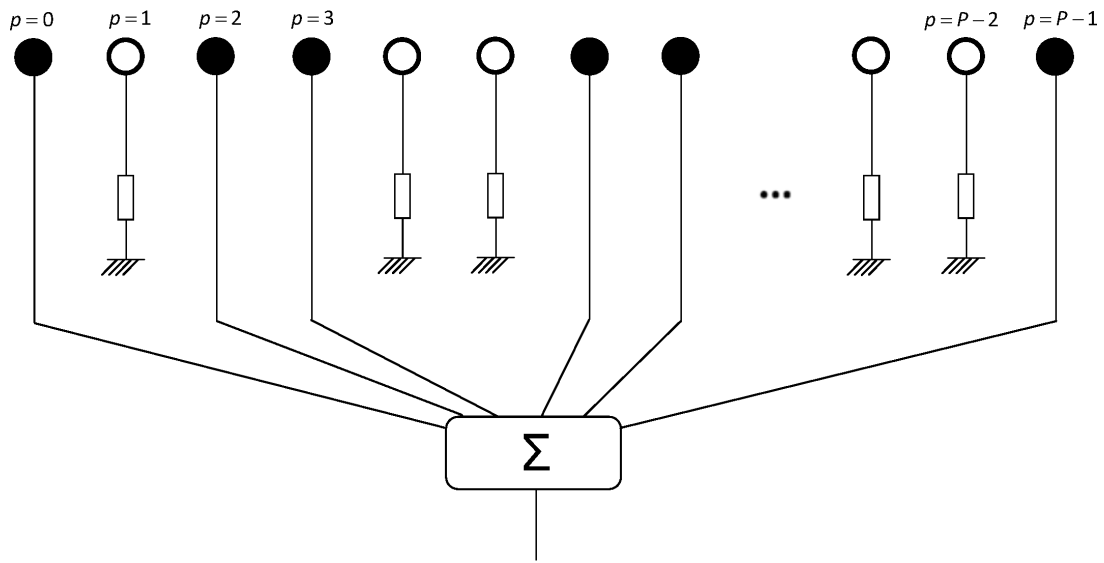
FIGURE CAPTIONS

- **Figure 1.** Sketch of (a) the TIA and (b) the flowchart of the GA-Based design process.
- **Figure 2.** *Proof of Concept* ($P = 16, \Delta z = 0.5\lambda, SLL = -15$ [dB]) - Relative frequency of the H ($H = 2^P$) cost function values: (a) PD and (b) AD formulations.
- **Figure 3.** *Illustrative Example* ($P = 24, \Delta z = 0.5\lambda, ADS$ Matching) - Plot of (a) γ_s^* , $\gamma_s(\hat{\alpha})$, and $\gamma_s(\alpha^{opt})$ ($s = 0, \dots, P - 1$), (b) $\Phi_{i_{conv}}^{best} |_{\nu}$ and $\rho(\hat{\alpha}_v, \alpha^{ADS})$ ($v = 1, \dots, V$; $V = 100$), (c) the parent layout, $\hat{\alpha}_v$ ($v = 1$), and (d) the final TIA, α_v^{opt} ($v = 1$).
- **Figure 4.** *Numerical Validation* ($P = 24, \Delta z = 0.5\lambda$, Flat Sidelobe Mask: $SLL = -15$ [dB]) - Plots of (a) $\mathcal{M}(u)$ and $\mathcal{E}^{feas}(u)$ along with the corresponding samples at $u = u_k$ ($u_k \triangleq \frac{\lambda}{P\Delta z}k$), $k = 0, \dots, P - 1$, and (b) the normalized target autocorrelation entries, $\gamma_s^*|^{ME}$ and $\gamma_s^*|^{FPE}$ ($s = 0, \dots, P - 1$).
- **Figure 5.** *Numerical Validation* ($P = 24, \Delta z = 0.5\lambda$, Flat Sidelobe Mask: $SLL = -15$ [dB], ME-AD Method) - Plots of (a) the iterative evolution of best cost function value, Φ_i^{best} ($i = 1, \dots, I$; $I = 50$), (b) the entries γ_s^* , $\gamma_s(\hat{\alpha})$, and $\gamma_s(\alpha^{opt})$ ($s = 0, \dots, P - 1$), and (c) the mask matching error of the cyclic sequences $\{\xi(\hat{\alpha}^{(\sigma)}); (\sigma = 0, \dots, P - 1)\}$.
- **Figure 6.** *Numerical Validation* ($P = 24, \Delta z = 0.5\lambda$, Flat Sidelobe Mask: $SLL = -15$ [dB], ME-AD Method) - Layouts of (a) the parent sequence, $\hat{\alpha}$, and (b) the final TIA arrangement, α^{opt} . Plots of (c) $\mathcal{M}(u)$, $\hat{\mathcal{E}}(u)$, $\mathcal{E}(u)$ and the corresponding samples at $\{u = u_k; k = 0, \dots, P - 1\}$.
- **Figure 7.** *Numerical Validation* ($P = 24, \Delta z = 0.5\lambda$, Flat Sidelobe Mask: $SLL = -15$ [dB], ME-AD Method) - Relative frequency of the H ($H = 2^P$) cost function values: (a) PD and (b) AD formulations.
- **Figure 8.** *Numerical Validation* ($P = 24, \Delta z = 0.5\lambda$, Flat Sidelobe Mask: $SLL = -15$ [dB], FPE-AD Method) - Plots of (a) the entries γ_s^* , $\gamma_s(\hat{\alpha})$, and $\gamma_s(\alpha^{opt})$ ($s = 0, \dots, P - 1$). Layouts of (b) the parent sequence, $\hat{\alpha}$, and (c) the final TIA arrangement, α^{opt} . Plots of (d) $\mathcal{M}(u)$, $\hat{\mathcal{E}}(u)$, $\mathcal{E}(u)$ and the corresponding samples at $\{u = u_k; k = 0, \dots, P - 1\}$.

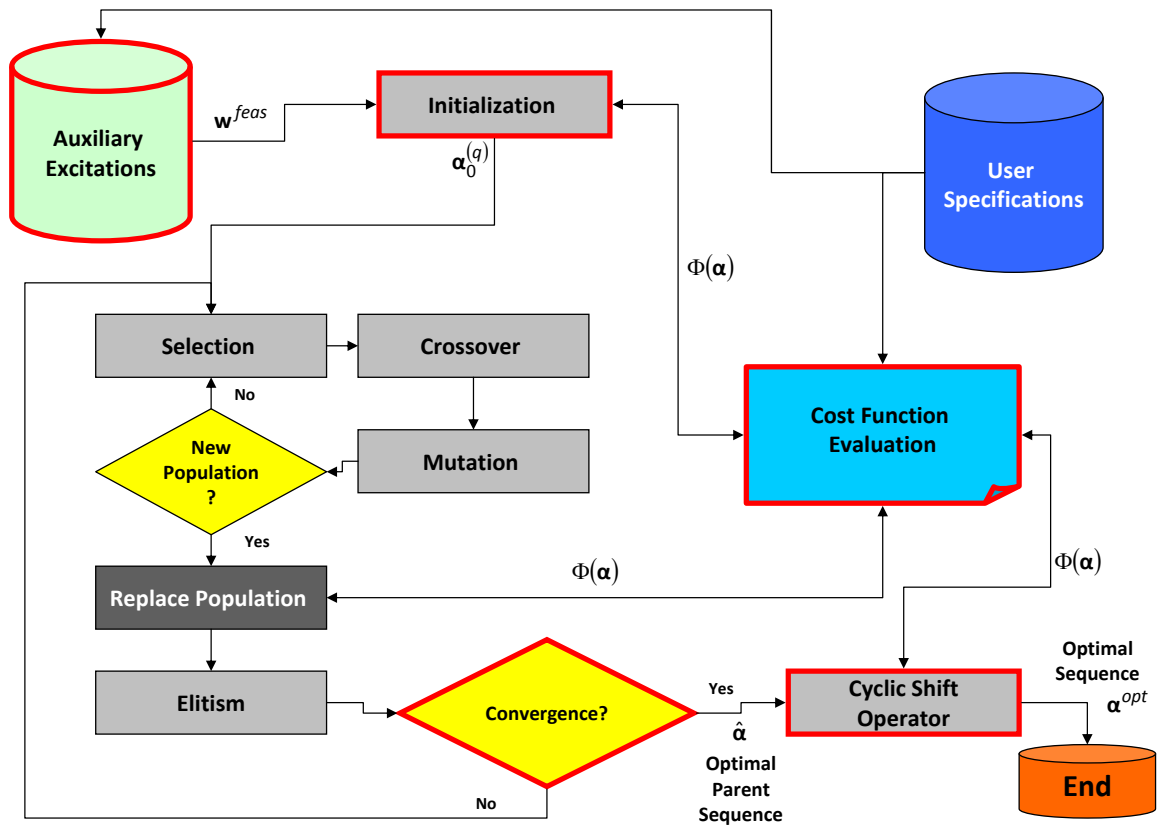
- **Figure 9.** *Numerical Validation* ($P = 24$, $\Delta z = 0.5\lambda$, Flat Sidelobe Mask, *AD* Formulation) - Behaviour of $\xi(\alpha^{opt})$ versus *SLL*.
- **Figure 10.** *Numerical Validation* ($P = 24$, $\Delta z = 0.5\lambda$, *FPE-AD* Method) - Layout of (a)(b) the final *TIA* arrangement, α^{opt} , and plots of (c)(d) $\mathcal{M}(u)$, $\widehat{\mathcal{E}}(u)$, and $\mathcal{E}(u)$ when enforcing (a)(c) the “Tapered” (*TM*) or (b)(d) the “Irregular” (*IM*) sidelobe mask.
- **Figure 11.** *Numerical Validation (Array Element)* - Picture of (a) the cavity-backed patch and (b) the corresponding embedded element pattern.
- **Figure 12.** *Numerical Validation* ($P = 24$, $\Delta z = 0.5\lambda$, *FPE-AD* Method) - Plots of (a)(b) the *HFSS*-simulated *3D* power pattern and (c)(d) $\mathcal{M}(u)$ and $\mathcal{E}(u)$ along the elevation cut when enforcing (a)(c) the “Tapered” (*TM*) or (b)(d) the “Irregular” (*IM*) sidelobe mask.
- **Figure 13.** *Numerical Validation* ($\Delta z = 0.5\lambda$, Irregular Mask [Type 2]) - Behaviour of (a) $\xi(\alpha^{opt})$ versus the aperture size (i.e., the number of array elements, P). Layout of the *TIA* arrangement synthesized with (b) the *PD*-based Method and (c) the *FPE-AD* one, α^{opt} , along with (d) the plots of $\mathcal{M}(u)$ and $\mathcal{E}(u)$ when $P = 48$.
- **Figure 14.** *Numerical Validation* (Irregular Mask [Type 2]) - Synthesis time, Δt , versus the aperture size (i.e., the number of array elements, P).

TABLE CAPTIONS

- **Table I.** *Numerical Validation (Array Element)* - Geometric and dielectric descriptors of the cavity-backed patch.



(a)



(b)

Fig. 1 - L. Poli et al., “Unconventional Array Design in the Autocorrelation Domain...”

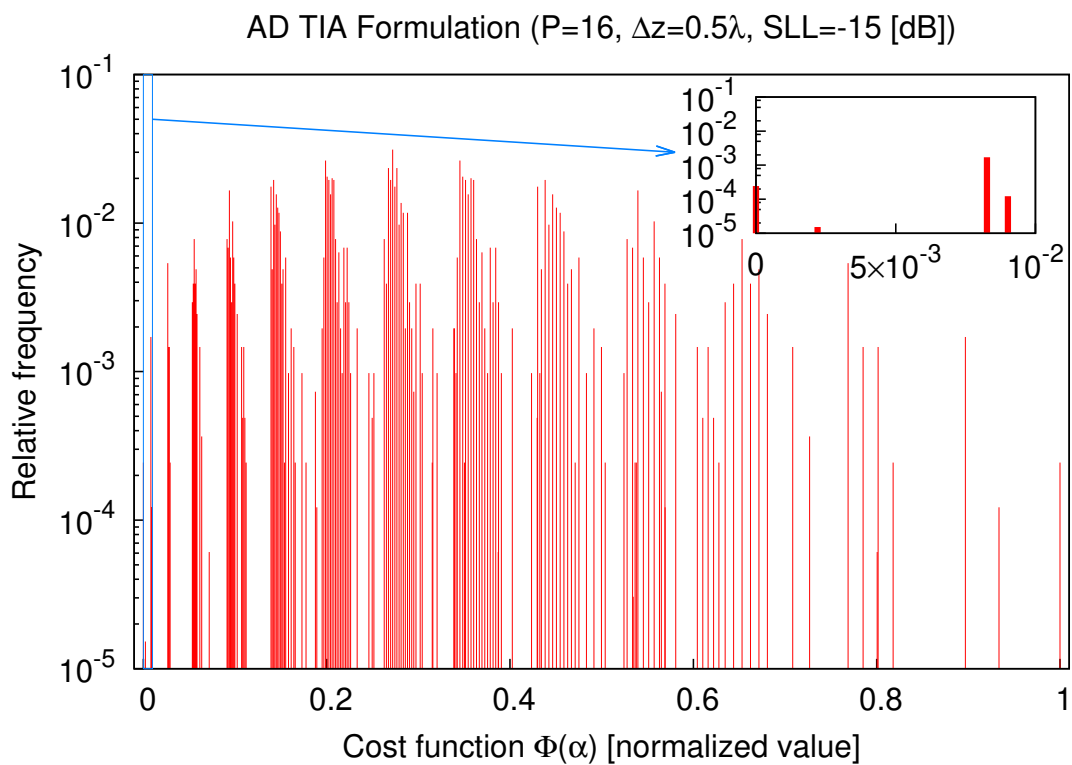
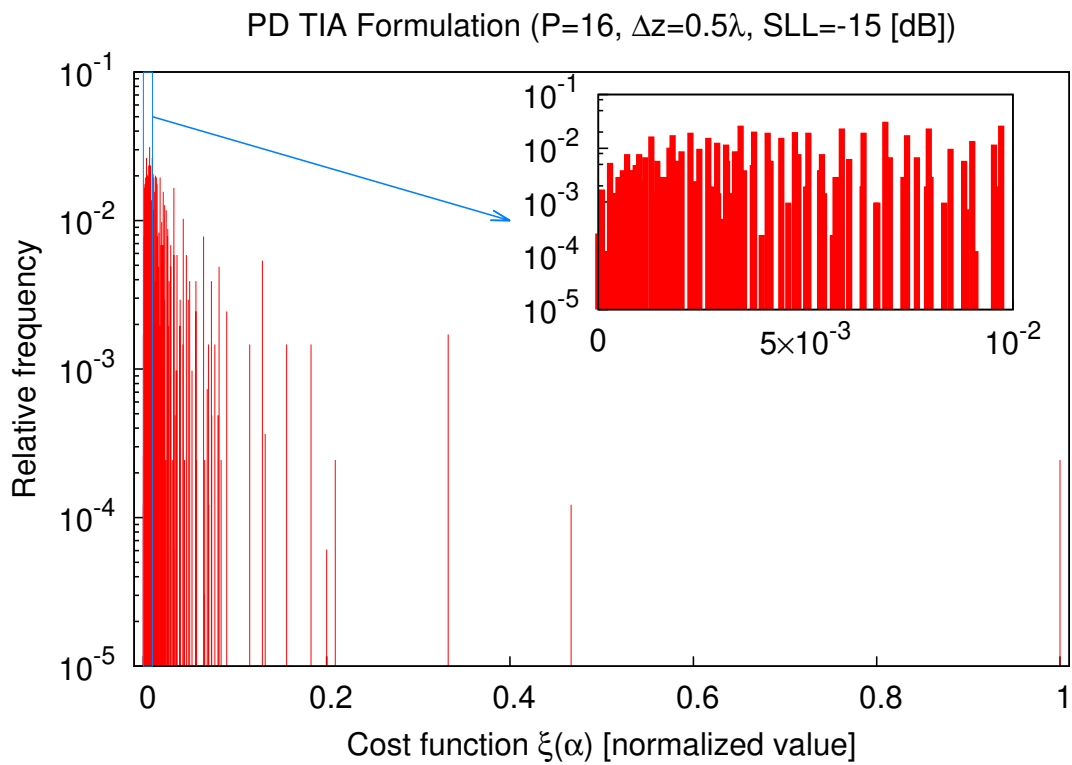


Fig. 2 - L. Poli et al., “Unconventional Array Design in the Autocorrelation Domain...”

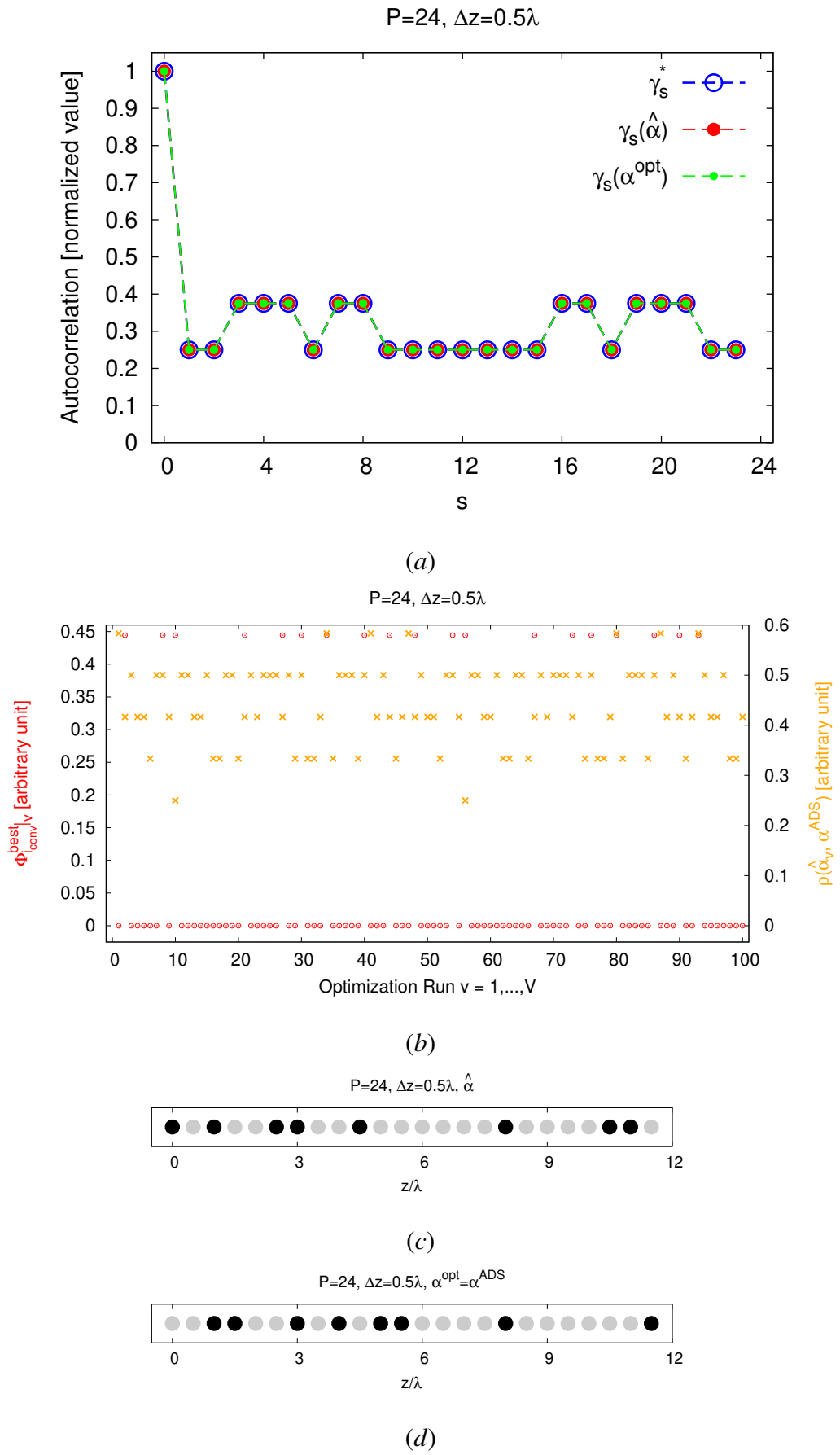
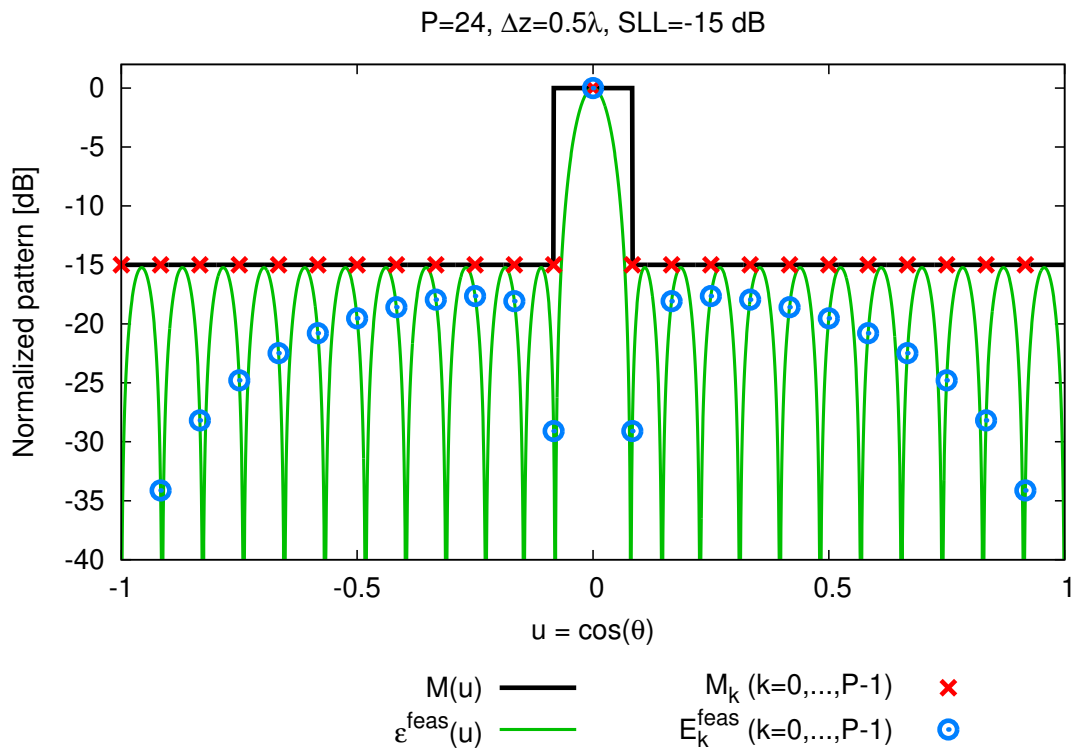
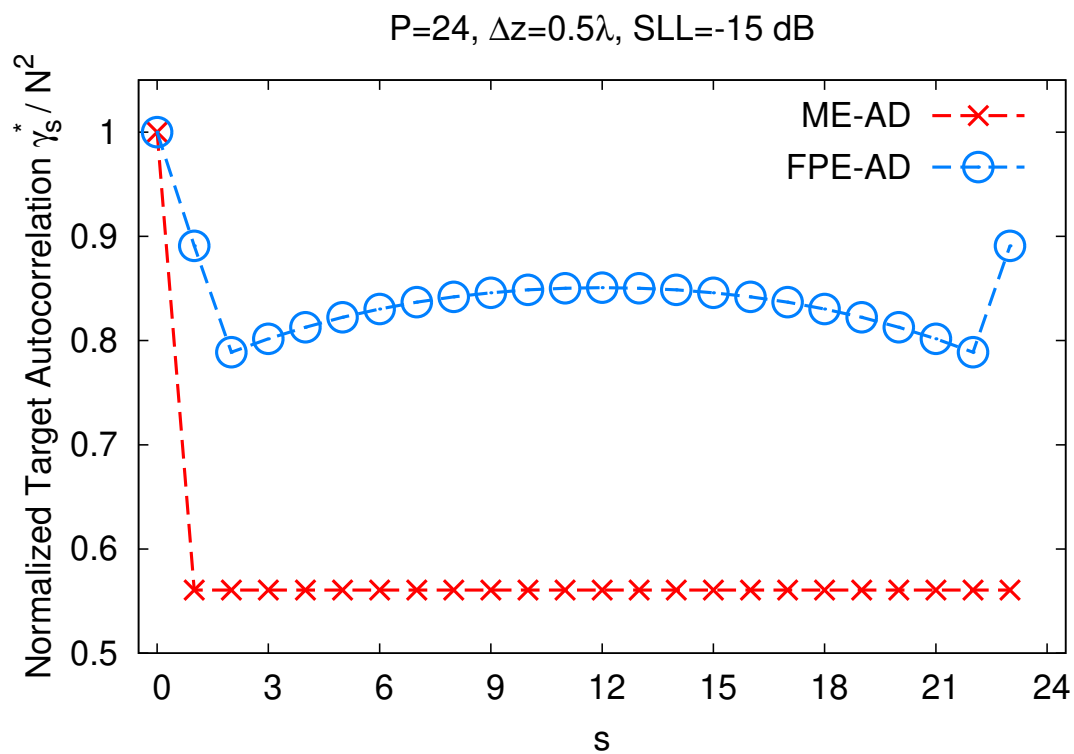


Fig. 3 - L. Poli et al., “Unconventional Array Design in the Autocorrelation Domain...”



(a)



(b)

Fig. 4 - L. Poli et al., “Unconventional Array Design in the Autocorrelation Domain...”

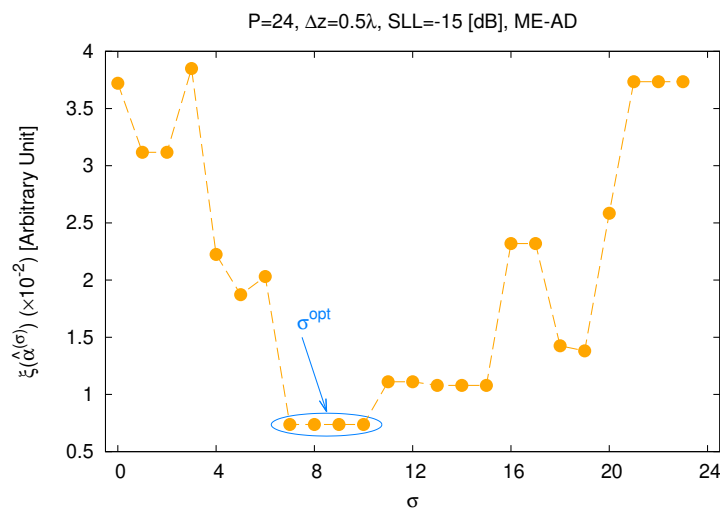
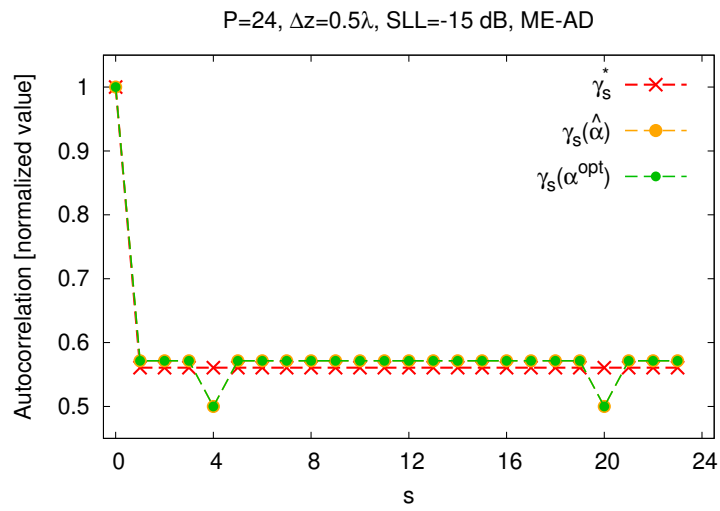
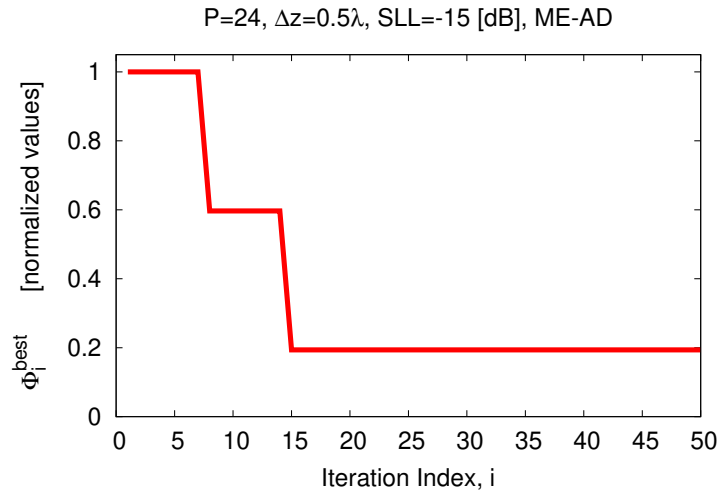
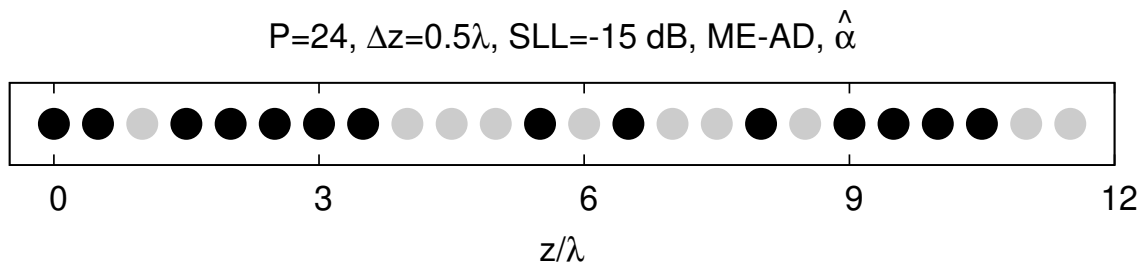
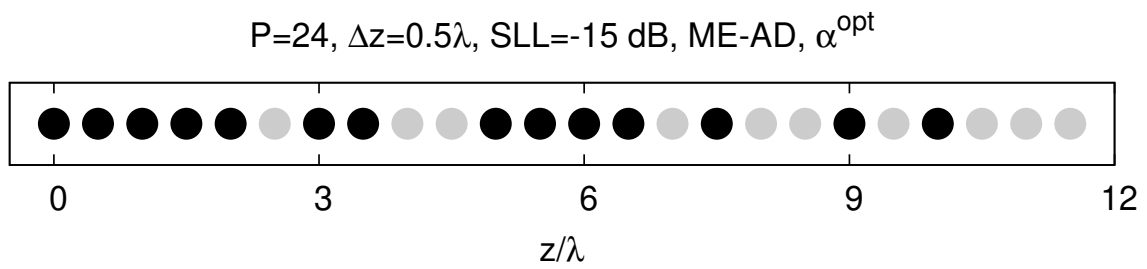


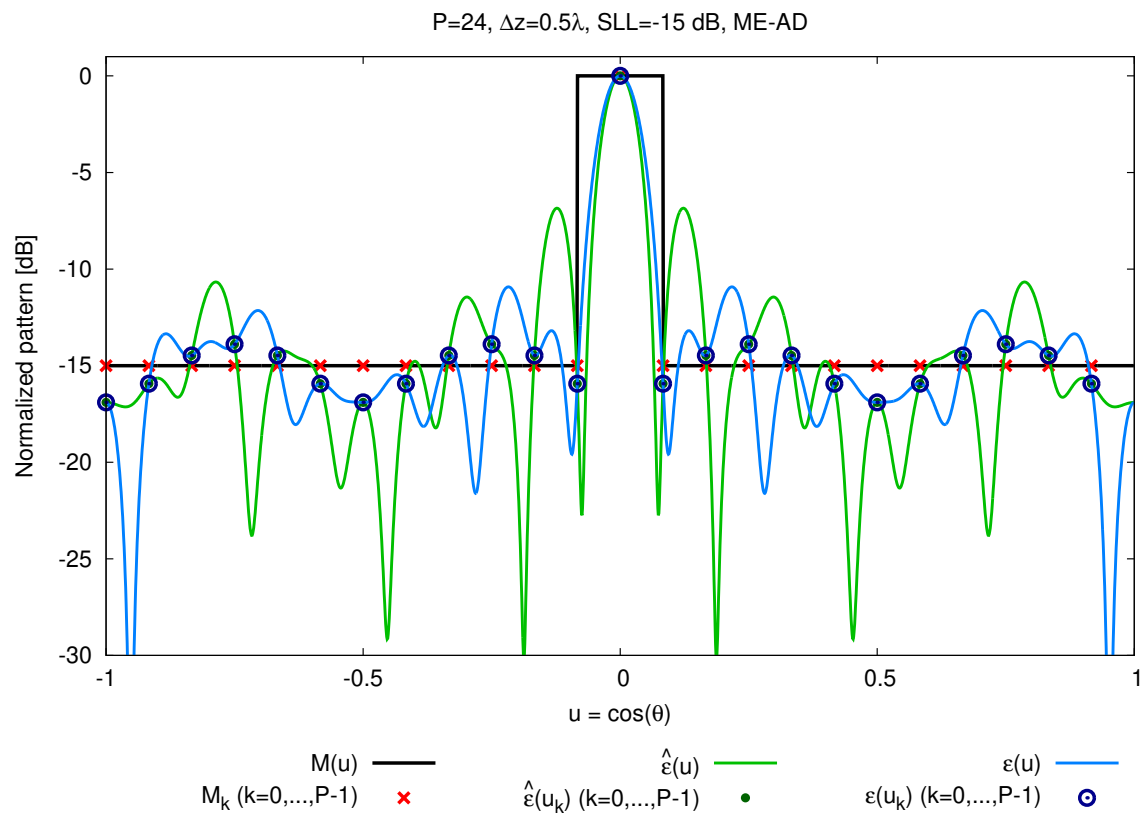
Fig. 5 - L. Poli et al., “Unconventional Array Design in the Autocorrelation Domain...”



(a)



(b)



(c)

Fig. 6 - L. Poli et al., “Unconventional Array Design in the Autocorrelation Domain...”

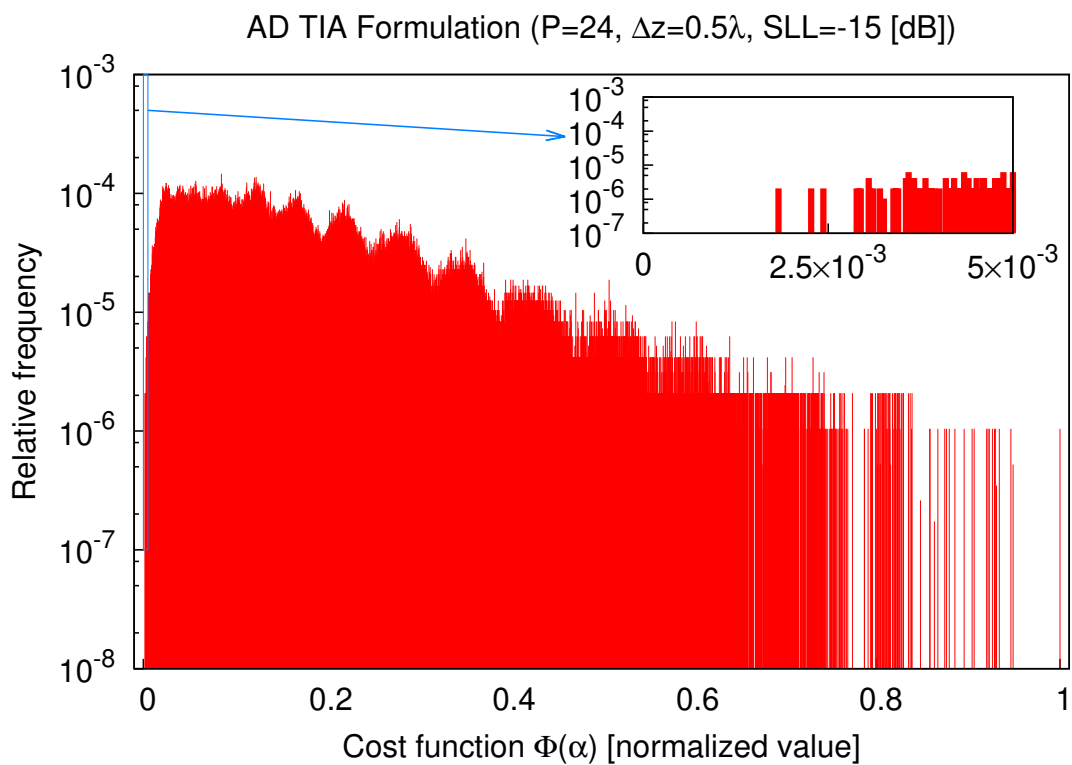
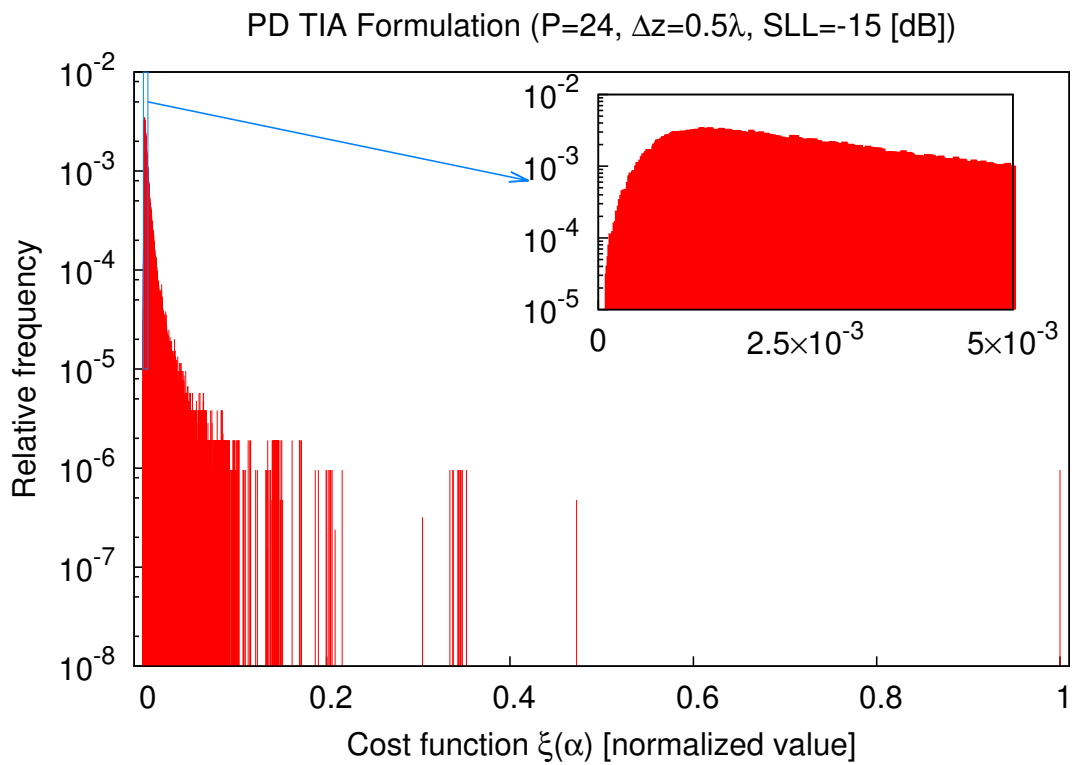


Fig. 7 - L. Poli et al., “Unconventional Array Design in the Autocorrelation Domain...”

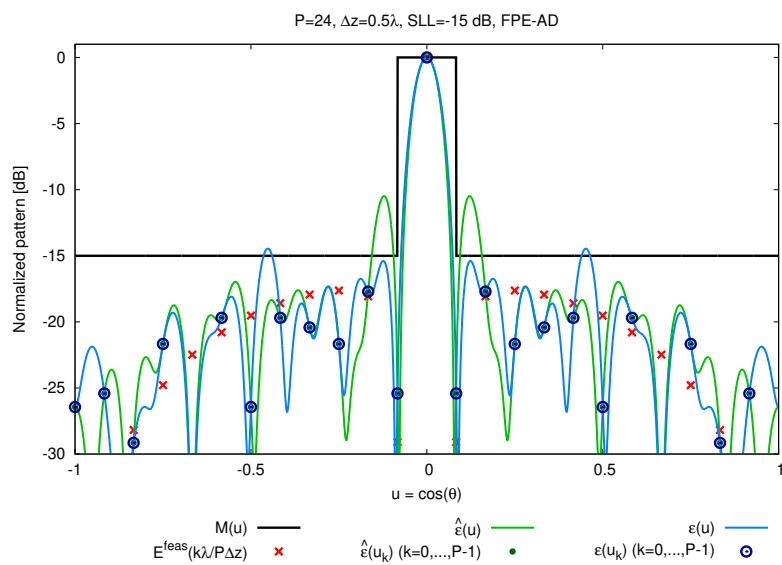
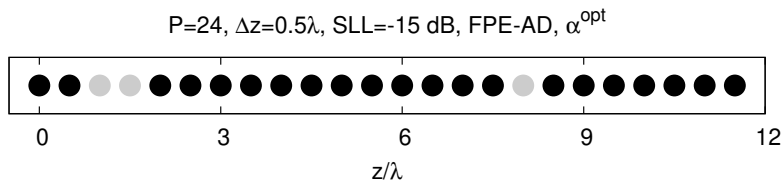
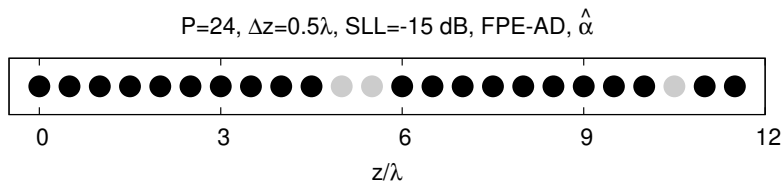
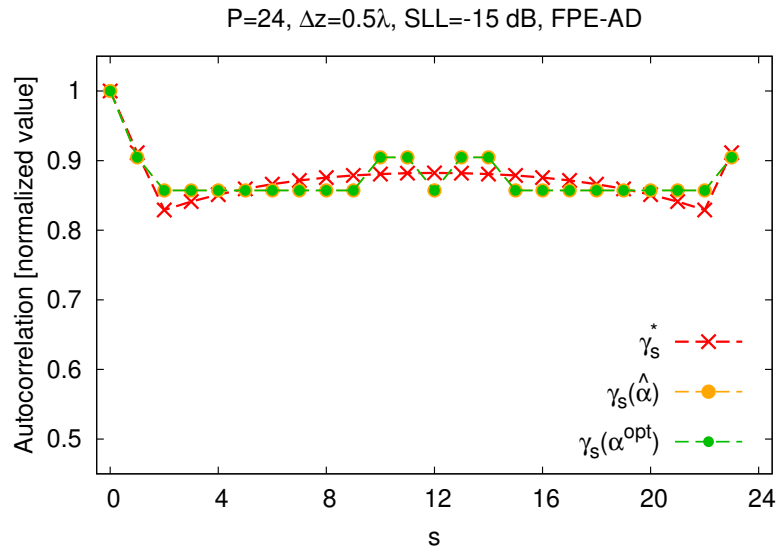


Fig. 8 - L. Poli et al., “Unconventional Array Design in the Autocorrelation Domain...”

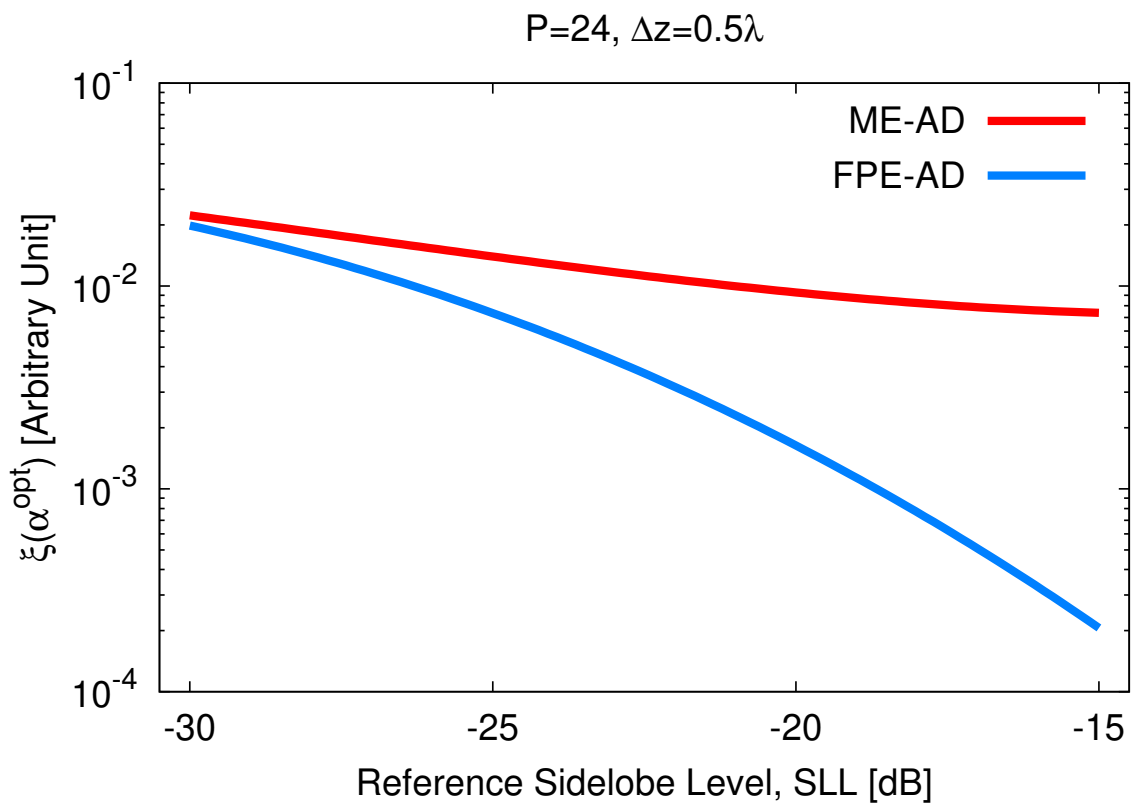


Fig. 9 - L. Poli et al., “Unconventional Array Design in the Autocorrelation Domain...”

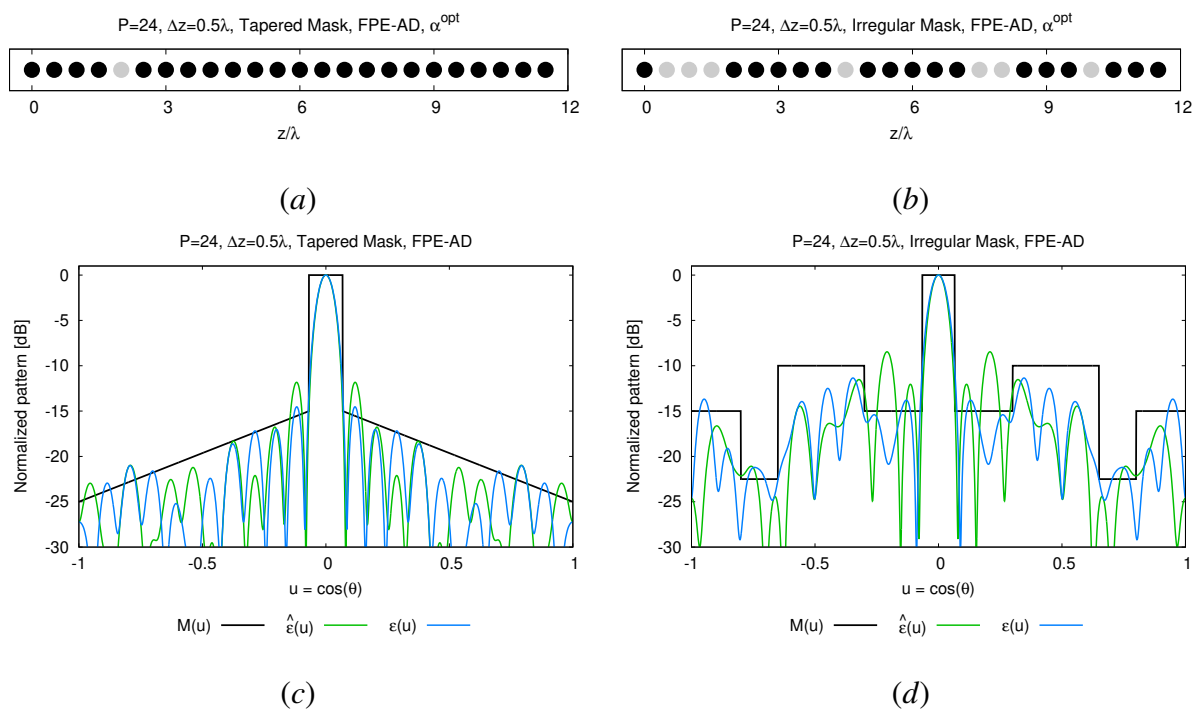
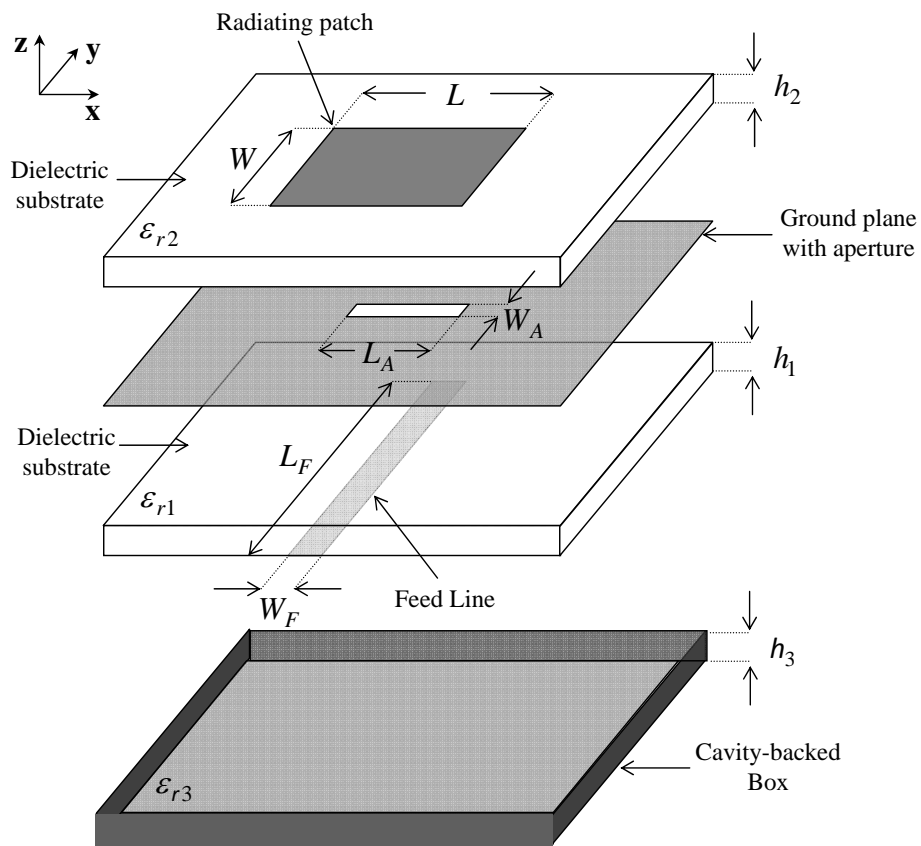
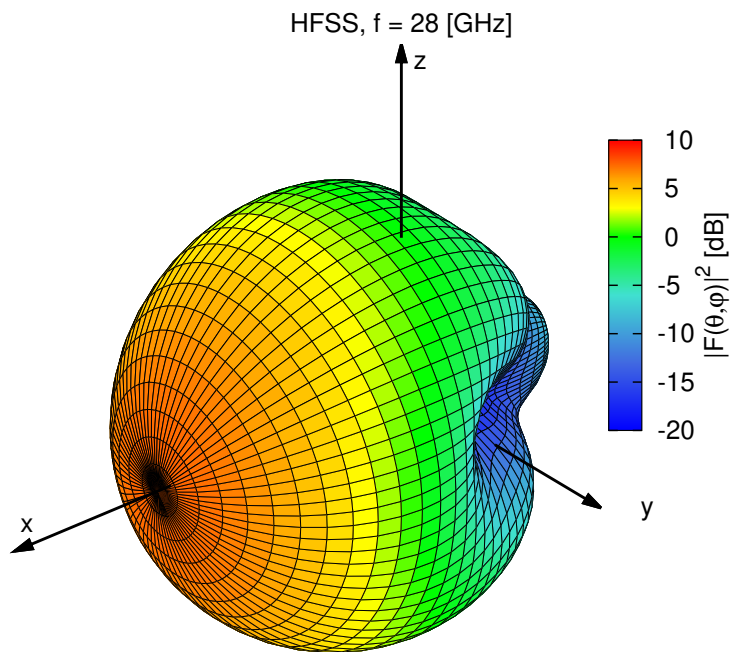


Fig. 10 - L. Poli et al., “Unconventional Array Design in the Autocorrelation Domain...”



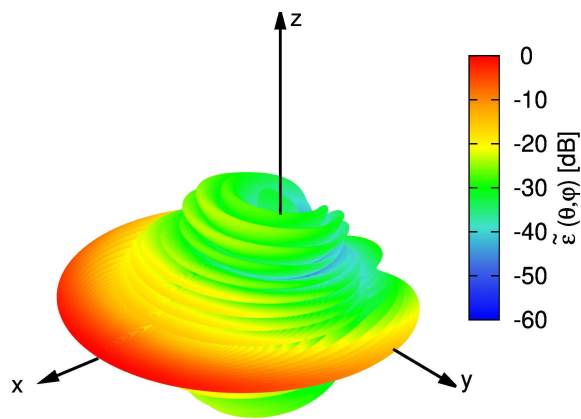
(a)



(b)

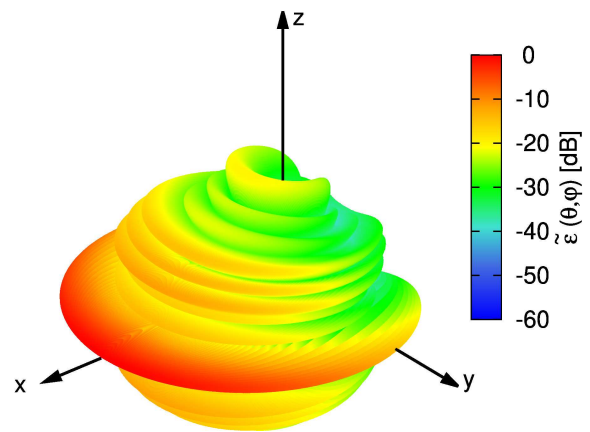
Fig. 11 - L. Poli et al., "Unconventional Array Design in the Autocorrelation Domain..."

P=24, $\Delta z=0.5\lambda$, Tapered Mask, FPE-AD, α^{opt} , HFSS



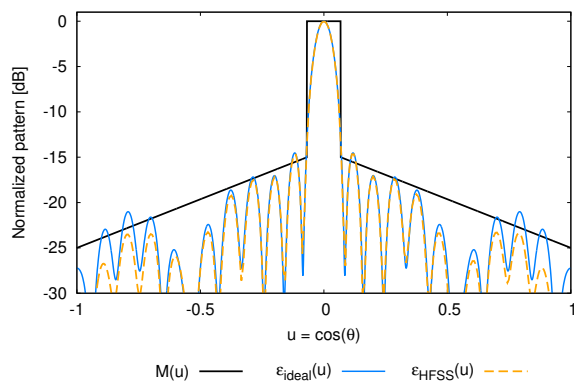
(a)

P=24, $\Delta z=0.5\lambda$, Irregular Mask, FPE-AD, α^{opt} , HFSS



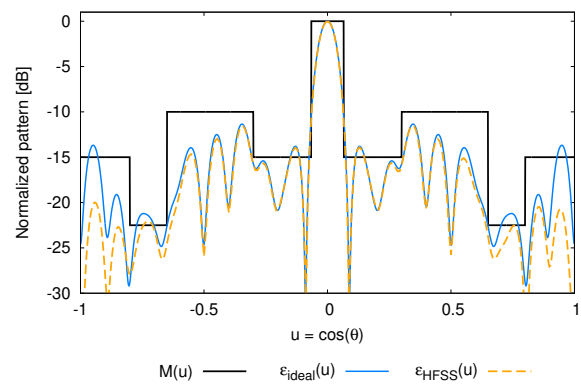
(b)

P=24, $\Delta z=0.5\lambda$, Tapered Mask, FPE-AD



(c)

P=24, $\Delta z=0.5\lambda$, Irregular Mask, FPE-AD



(d)

Fig. 12 - L. Poli et al., "Unconventional Array Design in the Autocorrelation Domain..."

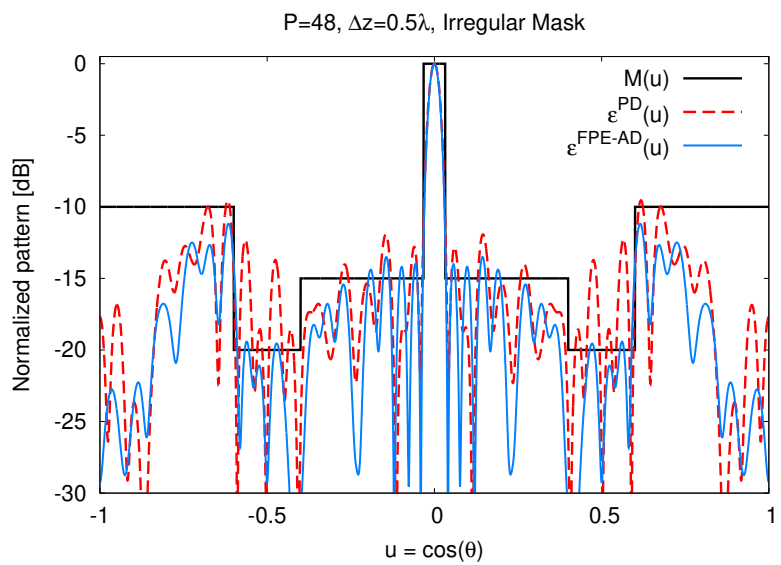
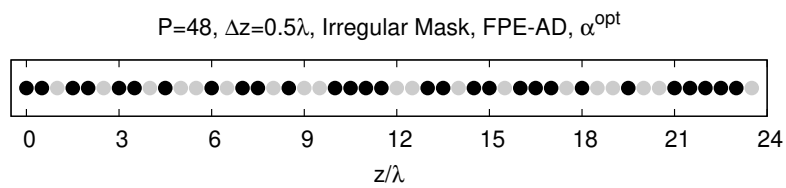
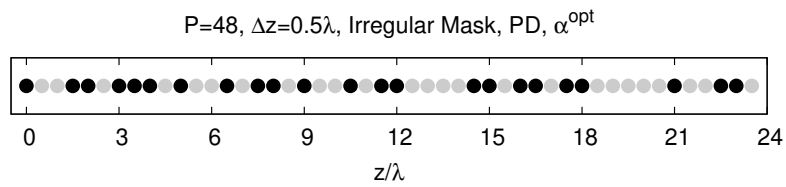
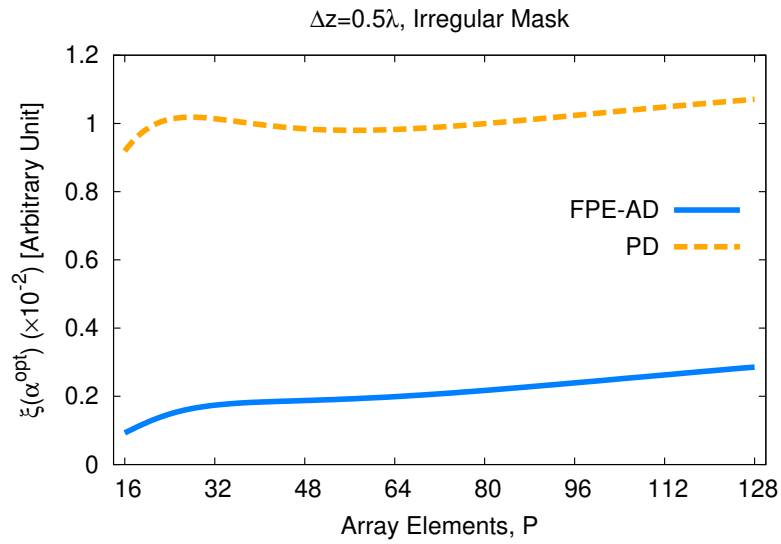


Fig. 13 - L. Poli et al., “Unconventional Array Design in the Autocorrelation Domain...”

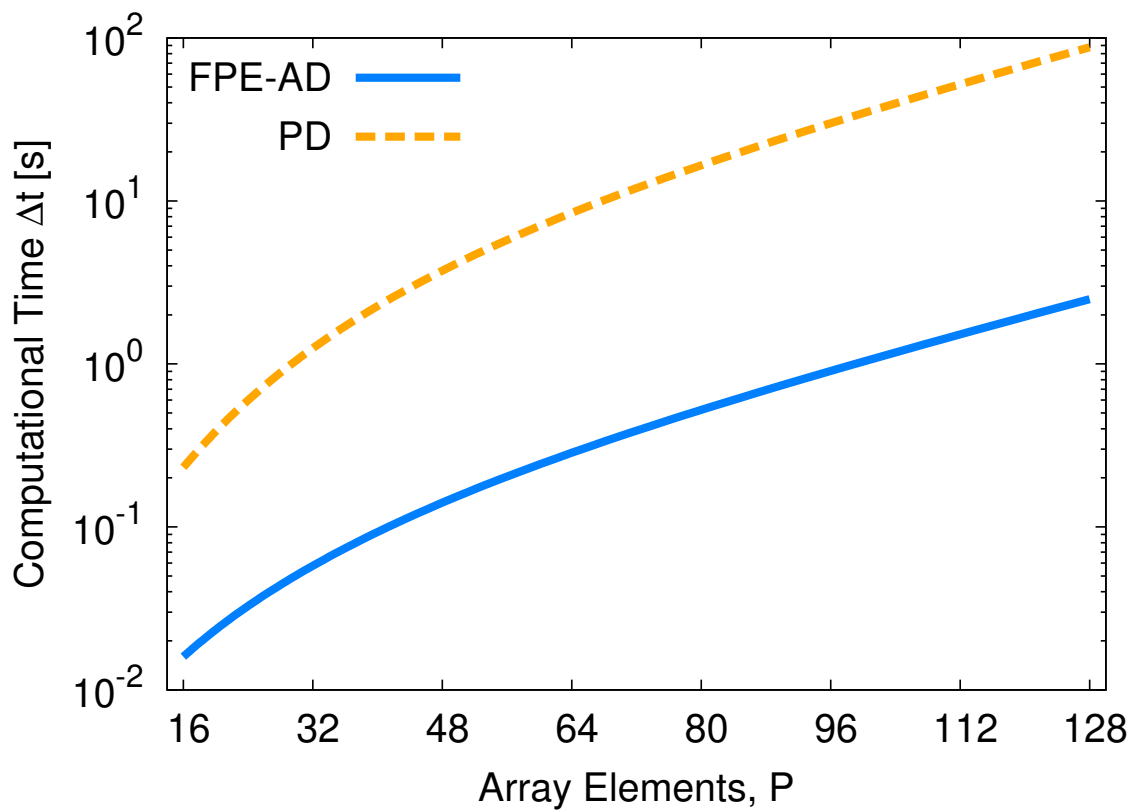


Fig. 14 - L. Poli et al., “Unconventional Array Design in the Autocorrelation Domain...”

<i>Geometrical Parameters</i> [mm]			<i>Electrical Parameters</i>
$W = 4.303$	$W_A = 2.151$	$W_F = 0.177$	$\varepsilon_{r1} = 2.1$
$L = 3.260$	$L_A = 0.323$	$L_F = 2.143$	$\varepsilon_{r2} = 2.1$
$h_1 = 0.627$	$h_2 = 0.070$	$h_3 = 1.563$	$\varepsilon_{r3} = 1.0$

Tab. I - L. Poli et al., “Unconventional Array Design in the Autocorrelation Domain...”